ELECTRODEPOSITION OF BLACK COBALT AS A SELECTIVE SOLAR ABSORBER COATING

by

John D. Bruno

ProQuest LLC.
789 East Eisenhower Parkway
P.O. Box 1346
Ann Arbor, MI 48106 – 1346

T-2296

A thesis submitted to the Faculty and the Board of Trustees of the Colorado School of Mines in partial fulfillment of the requirements for the degree of Master's of Science - Metallurgical Engineering.

Golden, Colorado

Date April 1, 1980

Signed: John D. Bruno
Student

Approved: William A. Averill
Thesis Advisor

Golden, Colorado

Date June 23, 1980

William D. Copeland
Head of Department

ABSTRACT

The development of the black cobalt plating process is described. By using a basic Watts cobalt bath with reduced boric acid and with the addition of an oxidant, good integrity black deposits could be obtained, by using appropriate operating conditions, that had suitable optical properties for use as a selective absorber coating. The black properties could be improved by increasing the oxidant concentration and/or the current density. Good adhering films could be obtained by operating in a specific current density range with proper agitation. Annealing changed the film thickness and the optical properties. The optimum operating conditions have been in an oxidant concentration range of .07 to .1 M nitric acid and a current density range of 1.20 - 1.60 kilo amps/m^2. Films obtained within these operating conditions have had good adherence and an after annealed solar absorbance of .91 to .93 with an infrared emittance of .10 to .20.

The use of black cobalt as a high temperature selective coating is discussed and future work is outlined.

TABLE OF CONTENTS

LIST OF FIGURES

LIST OF TABLES

LIST OF SYMBOLS

A	electrode area
C_o	concentration of reactant at electrode surface, mole/cm^3
C_B	concentration of reactant in bulk solution, mole/cm^3
D	diffusion coefficient, cm^2/sec
E	electric field intensity
F	Faraday's constant, coulomb/equiv
ΔG	Free energy of reaction, Joule/mole
ΔG_2, ΔG_2	activation energies, Joule/mole
i	normal current density of electrode surface, amp/cm^2
i_o	exchange current density, amp/cm^2
i_{ave}	average current density, amp/cm^2
i_L	limiting current density, amp/cm^2
I	total current to disk, amp
j	ion flux to electrode, mole/cm·sec
k	rate constant
L	length of Hull cell anode, cm
ℓ	shortest distance between electrodes in Hull cell
r	radial coordinate
r_o	radius of disk, cm
r_1, r_2	rates of forward and reverse reactions
R	universal gas constant, Joule/mole-deg
t	transport number of reactant
T	absolute temperature, ^oK
V	applied voltage, volt

w	width of Hull cell electrode, cm
y	distance along Hull cell cathode, cm
z	number of electrons transferred in reaction
α	transfer coefficient
β	symmetry factor
δ	mass transfer boundary layer thickness, cm
η	surface overpotential, volt
η_a	activation overpotential, volt
η_c	concentration overpotential, volt
ϱ	resistivity, ohm-cm
κ	conductivity, ohm^{-1}, cm^{-1}
θ	angle in Hull cell arrangement, deg
ν	kinematic viscosity, cm^2/sec
ϕ	electrostatic potential, volt
ϕ_o	external potential extrapolated to electrode surface, volt
ω	rotational speed, radiants/sec

ACKNOWLEDGEMENTS

This project was supported by the Solar Energy Research Institute and in part by the Kroll Institute for Extractive Metallurgy.

The author would like to express his gratitude to Dr. Patrick Call for his support of this project and especially to Roland Pitts, for all of his help, friendship and moral support.

The author would also like to thank Dr. William Averill, who was always available for counselling, who always treated the author as an equal, and who provided the space needed for personal growth and learning.

1. INTRODUCTION

The performance of solar photothermal power plants depends largely on the performance of the absorber coating. The absorber coating should absorb almost all of the solar radiation without losing its thermal energy through re-radiation of the heated surface, coatings that operate in this manner are called selective absorber coatings. Most of the incident solar energy lies in the wavelength interval of .35 μm to 2.2 μm and the energy radiated by a blackbody depends on the temperature but mainly lies in the infrared region with wavelengths greater than 1 to 2 μm. An "ideal" selective coating would be completely absorbing to wavelengths less than about 2 μm and be completely reflecting to wavelengths greater than 2 μm.

Tabor (1) has shown that one of the ways that a selective absorber coating may be obtained is by placing a thin absorbing material on a highly reflective substrate. In this way, the selectivity will depend on the coating thickness. The thickness of the coating should be great enough to obtain high absorption of the solar spectrum but still be thin enough so that it will be effectively transparent for the longer wavelengths allowing the reflectiveness of the metal substrate to dominate.

One of the most basic problems encountered with selec-

tive absorber coatings is stability at elevated temperatures. Studies done on electrodeposited black chrome (2) have shown that black chrome was unstable above 350°C. Many tests showed significant optical degradation of some of the coatings at 300° and 350°C, and more recent evidence indicates coating degradation in normal operation at about 100°C (3).

An early investigation by Kokoropoulous (4) indicated that black cobalt, (Co_3O_4) had reasonable absorbance and emittance properties and that it was stable up to 900°C. These films were prepared by electroplating metallic cobalt on to polished substrates of silver and platinum and then oxidized in air at 600°, 800°, 900° and 1100°C.

The purpose of this investigation was to further evaluate the use of black cobalt as a selective absorber coating for high temperature use and to check the feasibility of obtaining black cobalt through direct electrodeposition. Obtaining black cobalt directly from a plating bath would be highly desirable since it would eliminate the need for expensive furnace annealing of collector panels.

Several investigators (5-8) have studied the electrodeposition of metallic cobalt from various plating baths. Morral (9) has reviewed cobalt electroplating up to 1966. No work has been done on the plating of cobalt oxides except for some work done on the anodic formation of cobalt oxides (10-15). In a German patent application (16), a procedure

for depositing black cobalt is described in which cobalt is deposited as a sulfide at the cathode.

The work detailed here describes the development of the black cobalt plating system. After a bath composition was established, an attempt was made to correlate the deposit characteristics, such as integrity and optical properties, with the operating conditions, such as oxidant concentration, current density, bath composition, and agitation. Preliminary development was done in a Hull Cell, and later a rotating disk electrode arrangement was used in order to control the mass transfer boundary layer thickness and to allow a more accurate determination of current density distribution.

2. THEORETICAL CONSIDERATIONS

2.1 Hull Cell

The Hull Cell, shown in Figure 1, allows one to obtain a large variation in current density over the cathode surface. This variation is due to the increasing ohmic resistance between the electrode as the distance between the anode and cathode increases.

The resistivity, e, of the solution is given by:

$$e = \frac{R}{x} A \qquad (1)$$

where:

R is the total resistance to the electrode

A is the area of the electrode

x is the distance between the electrodes

The current density is given by:

$$i(x) = \frac{V_o}{R_{(x)} A} = \frac{V_o}{e} \qquad (2)$$

Which leads to an expression for the current density at any point x:

$$i(x) = V_o / e \ (\ell_o + x \tan \theta) \qquad (3)$$

Solving for the total current, I, yields:

$$I = \int_S i(x) \, dA$$

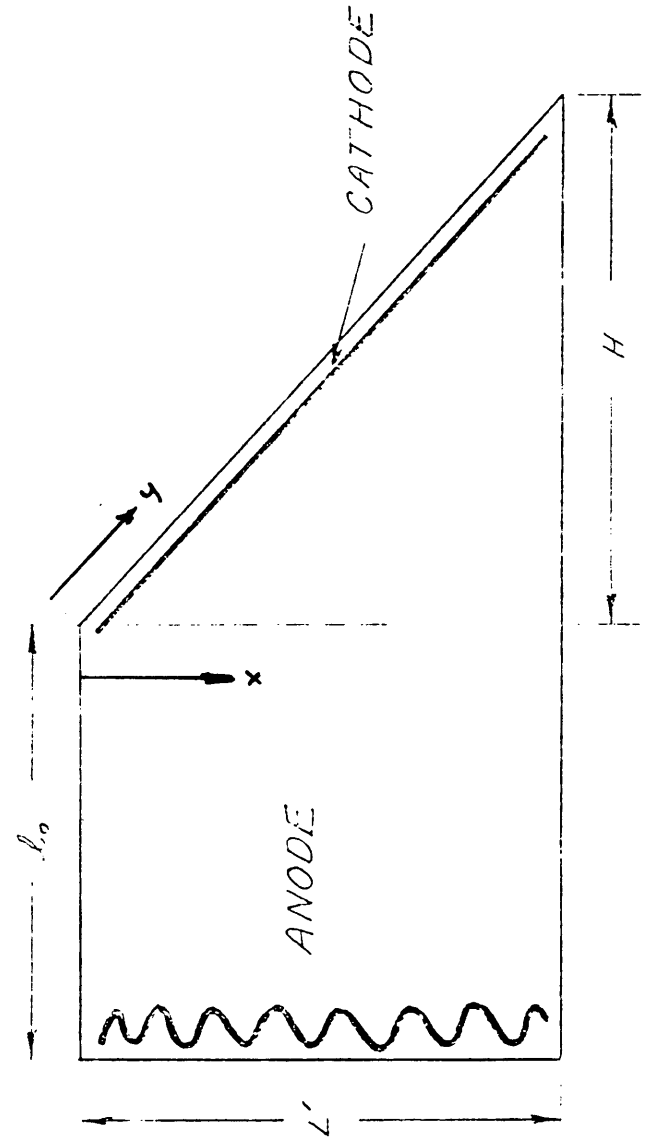

FIGURE 1. HULL CELL ARRANGEMENT

$$= \frac{V_o W}{e} \int_0^L \frac{dx}{\ell_o + \tan \theta}$$

$$= \frac{V_o w}{e} \ln \left(1 + \frac{L}{\ell_o} \tan \theta\right) \quad (4)$$

Combining Equations 3 and 4, one obtains a relationship for the local current density in terms of the total current and the cell geometry:

$$i(x) = \left(\frac{I}{w}\right) / \left(\ell_o + \tan \theta\right) \cdot \ln \left(1 + \frac{L}{\ell_o} \tan \theta\right) \quad (5)$$

Equation 5 can now be put in terms of the linear distance y along the cathode:

$$i(y) = KI/(\ell_o + y \sin \theta) \quad (6)$$

where:

$$K = 1/w \cdot \ln \left(1 + \frac{L}{\ell_o} \tan \theta\right)$$

In this way, the Hull Cell can be used as a useful tool in correlating deposit characteristics with local current density. However, the Hull Cell is limited in its interpretation because it neglects the edge effects encountered due to the discontinuity of the potential and it also assumes negligible activation and concentration over potentials.

2.2 Background on Transport in a Plating Cell

In a plating cell, several mechanisms compete simult-

taneously to impede the flow of metal ions, and the properties of the deposit depend on which of these mechanisms predominates. Obtaining suitable deposits is possible only if the dominant mechanism is known, since each is affected by different operating parameters.

The three mechanisms that limit transport are: ohmic - the bulk electrolyte resistivity; kinetic - the rate of the chemical reactions at the electrodes; and mass transport - a limitation due to the concentration gradients that develop near the electrode. Determining the current voltage relationships from each mechanism is a valid description of transport in a plating cell since, in a plating cell, for an individual reaction, these mechanisms operate in series. Therefore, the sum of all the voltages required to overcome these resistances is the applied voltage and the currents from each mechanism must be identical since the current is continuous and single valued.

The current/voltage relationship for ohmic control is described by Ohm's Law.

$$\underline{i} = \kappa \underline{E} \qquad (7)$$

Where $\underline{i}$ is the current density vector, is the bulk conductivity and $\underline{E}$ is the electric field intensity vector.

The electric field intensity, E, is dependent on the spatial distribution of the electric potential $\emptyset$, through

the relationship:

$$E = -\nabla \phi \tag{8}$$

In order to find the current distribution under ohmic control, which is referred to as the primary distribution, one must find an expression for the electric potential, which is accomplished by solving Laplace's differential equation:

$$\nabla^2 \phi = 0 \tag{9}$$

with the boundary conditions

ϕ = V applied, at the anode

ϕ = 0 at the cathode

i = 0 at insulators

Ohmic control usually predominates at low voltages and depends only on the cell geometry and the bulk electrolyte resistivity.

The kinetic resistance that is encountered at the electrode-electrolyte interface is a result of the energy needed to overcome the activation energy barrier due to adsorption and charge transfer. This is schematically indicated in Figure 2.

An atom must process an energy ΔG_1, called the activation energy, in order to potentially ionize, and a charge atom must have an activation energy ΔG_2, in order to discharge. The difference, ΔG, between the two creates an

internal voltage on the electrode, called its characteristic or equilibrium potential. This potential depends on the electrode involved, the concentration of ions, the solution, and the temperature.

The rates of ionization and discharge are expressed as:

$$r_1 = K_1 \exp (- \Delta G_1/RT) \quad (10)$$

$$r_2 = K_2 \exp (- \Delta G_2/RT) \quad (11)$$

At equilibrium, the rates in the forward and reverse directions are equal ($r_1 = r_2 = r_o$) and the electrode assumes its equilibrium potential given by:

$$E_o = - \Delta G/\not{Z} F \quad (12)$$

Where E_o is the equilibrium potential, $\not{Z}$ is the number of electrons transferred, and F is Faraday's constant.

The voltage in the current voltage relationships for each mechanism is called an overpotential indicating that the potential is in excess of the equilibrium electrode potential and emphasizing that plating is a non-equilibrium reaction.

Applying a voltage to the electrode enhances one process and impedes the other. Thus applying an overpotential adjusts the energy diagram as shown in Figure 3.

The expressions for the rates now become:

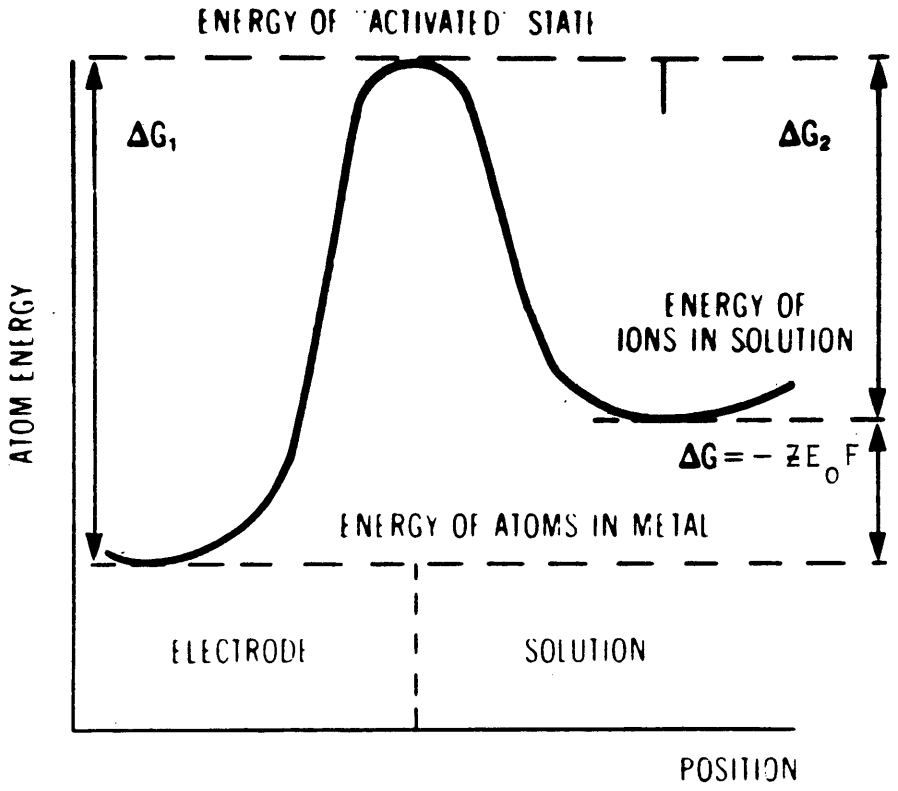

FIGURE 2. ENERGY BARRIER FOR A REVERSIBLE ELECTRODE

$$r_1 = r_o \exp (\alpha \nu \eta \quad F/RT) \tag{13}$$

$$r_2 = r_o \exp - (1-\alpha)\nu \eta \; F/RT) \tag{14}$$

where α is the transfer coefficient and represents the fraction of the applied energy that reduces the effective barrier for ionization, and the remaining fraction $(1-\alpha)$ applies to increasing the barrier to discharge.

The observable current, proportional to the difference between these rates is then given by the Butler-Volmer equation:

$$i = i_o \exp (\alpha \; \nu \eta \; F/RT) - i_o \exp (-(1-\alpha) \; \nu \eta \; F/RT)$$

where i_o is the equilibrium or exchange current density.

In most practical cases, the applied voltage is high enough that the reaction is forced far enough from equilibrium that one term predominates. The current voltage relationship then simplifies to the Tafel equation:

$$i = i_o \exp (\alpha \nu \eta \quad F/RT) \tag{15}$$

$$\eta = a + b \; \ln i \tag{16}$$

where:

$$a = - \frac{RT}{\alpha \nu F} \; \ln i_o$$

$$b = \frac{RT}{\alpha \nu F}$$

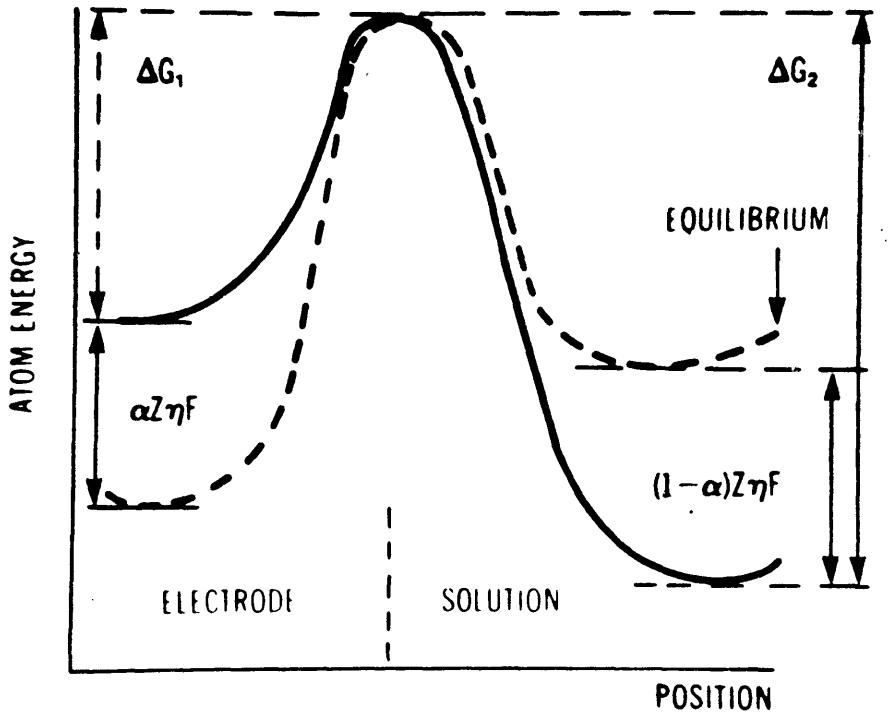

FIGURE 3. ENERGY BARRIER WITH A VOLTAGE, η, APPLIED TO AN ANODE

The overpotential required to overcome the kinetic resistance is called the activation overpotential and can be regarded as the result of imposing an additional resistance at the electrode interface. As a result, the electrolytic solution near the electrode is no longer an equipotential surface, and the current distribution obtained is called the secondary current distribution. The general effect of electrode polarization is to make the secondary current distribution more nearly uniform than the primary distribution, and an infinite current density at the edge of the electrodes is eliminated.

The mass transport resistance is a limitation due to the concentration gradients that develop near the electrode. Since the plated ions are consumed at the electrode faster than they are supplied by electrical migration, a region depleted of the plated ions is established near the electrode. This region is called the mass transfer or diffusion boundary layer, and is shown in Figure 4.

The ions to be plated are supplied to the cathode by migration and by diffusion across the concentration gradient according to the Nernst-Planck equation:

$$j = - \frac{Dc}{RT} z F \frac{d\phi}{dx} - D \frac{dc}{dx} \qquad (17)$$

Where j is the flux of plated ions, D is the diffusion

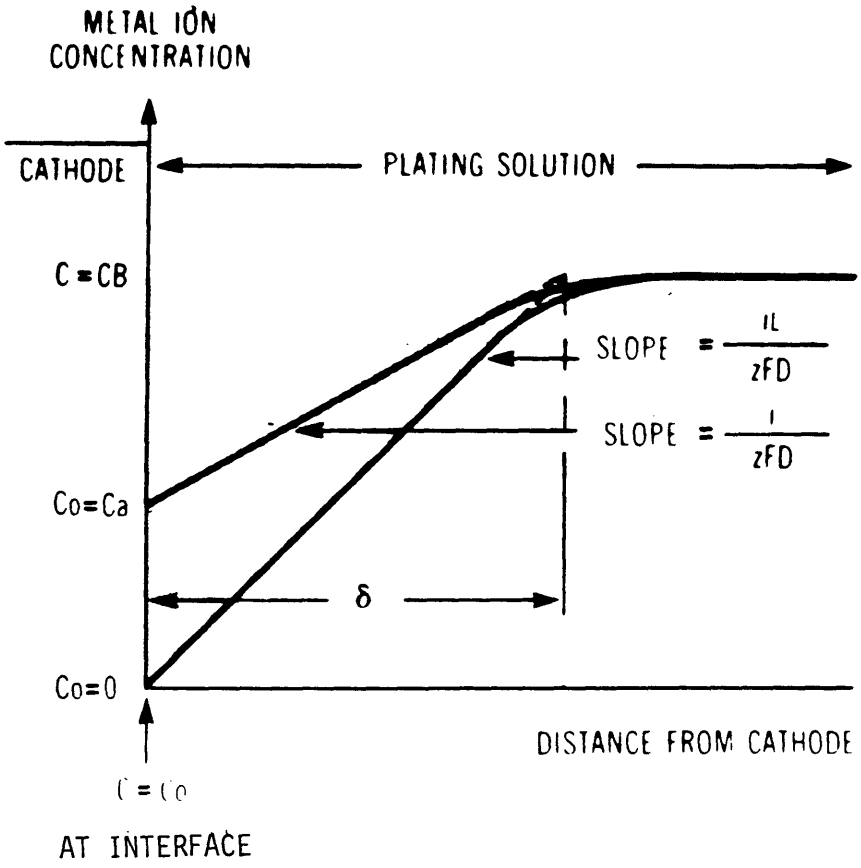

FIGURE 4. CONCENTRATION GRADIENT NEAR A CATHODE

coefficient of the ions, $\frac{dc}{dx}$ is the concentration gradient perpendicular to the electrode and $\frac{d\phi}{dx}$ is the gradient of electrostatic potential perpendicular to the electrode.

For the deposition of metal cations, the migration effect enhances the overall transport to the electrode surface. However, when the deposition process involves anions, as in the case of the electrodeposition of silver from silver cyanide ions, the effect of migration impedes the overall transport of ions to the electrode surface. In this case, transport to the cathode is achieved when the flux due to diffusion is larger than the flux due to migration.

The magnitude of the flux due to migration depends on the fraction of the current density carried by the electron-acceptor species undergoing charge transfer. This fraction is called the transport number, t, and is a function of the concentrations and mobilities of all the charged species in solution.

Assuming a linear concentration profile, one can obtain an expression for the current in terms of the bulk concentration, C_B, the concentration of the electrode surface, C_o, and the thickness of the diffusion boundary layer, δ, and the transport number:

$$i = - \frac{DzF}{1-t_+} \quad \frac{C_B - C_o}{\delta} \quad \text{(for cations)}$$

or:

$$i = -\frac{D\nu F}{1+t_-} \quad \frac{C_B - C_o}{\delta} \qquad \text{(for anions)} \qquad (18)$$

Most practical plating solutions have a large concentration of supporting electrolyte, thereby reducing the transport number to a negligible value.

At limiting current, that is, when the current is limited by the transport of ions to the electrode surface, the concentration of ions at the surface approaches zero and the expression for the current becomes:

$$i_L = \nu F D \frac{C_B}{\delta} \qquad (19)$$

The overpotential in diffusion-limited transport is related to the concentration through the Nernst equation:

$$\eta_c = \frac{RT}{\nu F} \ln \left(\frac{C_o}{C_B}\right) \qquad (20)$$

Since the concentrations can be related to the current by the relationship:

$$\frac{C_o}{C_B} = 1 - \frac{i}{i_L} \qquad (21)$$

One can obtain the concentration overpotential in terms of the current:

$$\eta_C = \frac{RT}{\nu F} \ln \left(1 - \frac{i}{i_L}\right) \qquad (22)$$

The effects of concentration overpotential can be minimized by increasing the reactant concentration, by agitating the solution and thereby reducing the mass transfer boundary layer and by increasing the temperature.

2.3 Rotating Disk Electrode

In order to control the factors that affect the deposit, it is convenient to use a rotating disk electrode system because the hydrodynamic and transport characteristics are well defined. A rotating disk system is shown in Figure 5 and consists of a disk electrode embedded in a larger insulating plant which rotates about its axis. This system has been reviewed by Riddiford (17).

The attractive aspects of the rotating disk electrode are that the fluid velocity normal to the disk is a function of the normal distance from the disk but not on the radial distance. Because of this, one obtains a uniform mass transfer boundary layer over the entire surface of the electrode. The solution of basic fluid flow equations results in an expression for the thickness of this laminar boundary layer, δ, as a function of the kinematic viscosity of the fluid, ν, and the angular velocity, ω, of the disk:

$$\delta \sim 2.8(\nu/\omega)^{\frac{1}{2}} \qquad (23)$$

If the diffusion coefficient of the reactant is known

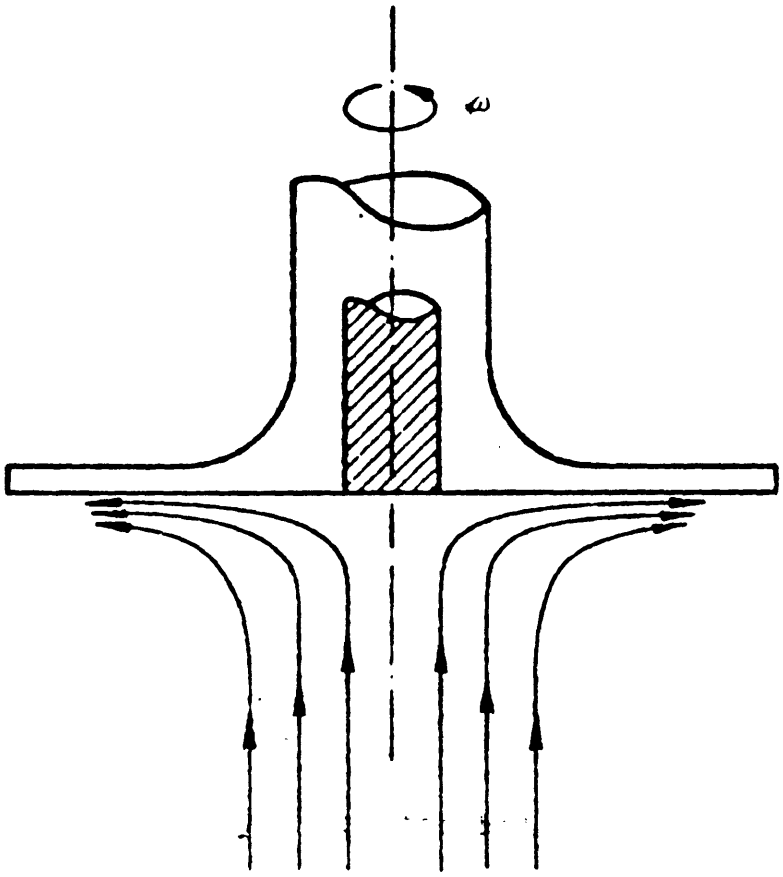

FIGURE 5. ROTATING DISK ELECTRODE

along with its bulk concentration one can obtain a good approximation for the limiting current:

$$i_L = .357\ \nu FD\ C_B\ (\omega/\nu)^{\frac{1}{2}} \qquad (24)$$

This expression assumes a linear concentration gradient while a more precise treatment would show that the concentration gradient is also a function of the diffusion coefficient and the kinematic viscosity. Taking this into consideration Levich (16) has shown that the limiting current is given by the expression:

$$i_L = \pm .620\ \nu FD^{2/3}\ \nu^{-1/6}\ \omega^{1/2}\ C_B \qquad (25)$$

This equation holds true when the electrolyte contains no more than three ion species. For more than three species the numerical constant will be somewhat less than .620 and must be determined empirically.

When the rotating disk electrode is operated below the limiting current one obtains a non-uniform current density across the radius of the disk as a result of the ohmic potential drop in the solution. The problem of the current distribution on a rotating disk operating below the limiting current has been treated by Newman (19) and his results will be summarized here.

For the primary current distribution, the surface of the electrode is considered to be an equipotential surface.

LaPlace's equation is solved by conformal-mapping using the Schwarz-Chistoffel transformation. The current and potential lines for a disk electrode are shown in Figure 6.

As a result, the current density on the disk for the primary distribution is:

$$i = .5\, i_{ave} / 1 - (r/r_o)^2 \qquad (26)$$

and the total current is:

$$I = 4\, \kappa_\beta\, r_o\, \phi_o \qquad (27)$$

where:

κ_β is the bulk conductivity

r_o is the disk radius

I is the total current

i is the local current density

i_{ave} is the average current density

ϕ_o is the external potential extrapolated to the electrode surface

In the case of primary current distribution, the surface overpotential and the concentration overpotential are negligible, and the current distribution is completely determined by the ohmic drop in the solution, with the result that the current density is infinite at the edge of the disk and is half of the average value at the center of the disk.

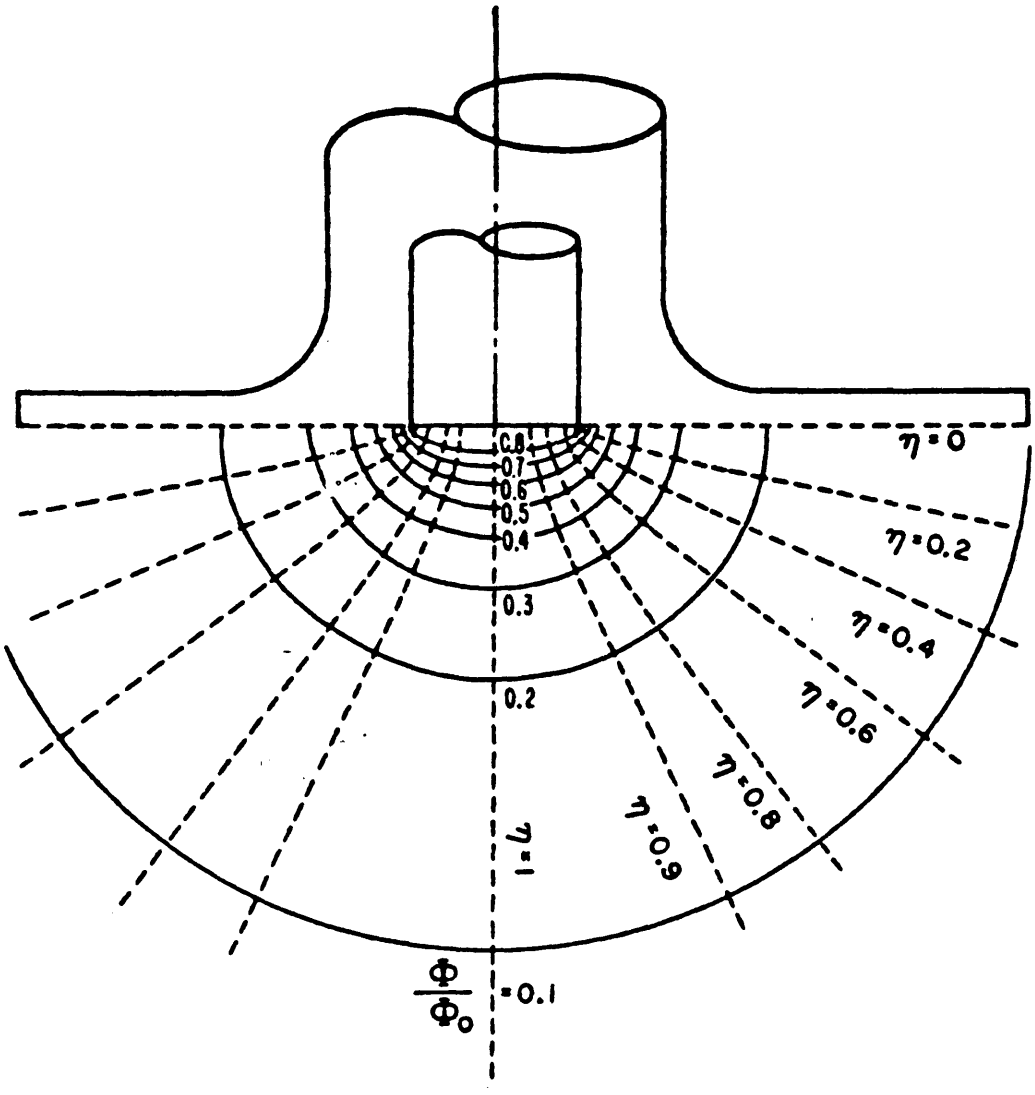

FIGURE 6. CURRENT AND POTENTIAL LINES FOR A DISK ELECTRODE

When the disk is operated at limiting current, a uniform current density is obtained. However, for the same total current, the current density at the center of the disk is twice as high as the primary current, and this requires a potential 27.3% higher in order to force the higher current density to the center of the disk. Also the potential at the edge of the disk is lower than for the primary distribution. This relationship for uniform current and uniform potential is shown in Figure 7.

If the rotation speed is high, so that $/i/<</i_{LIM}/$, then the concentration overpotential is negligible and the secondary current distribution is obtained. The secondary current distribution is determined by the balance between the activation overpotential and the ohmic drop in the solution.

When $/i/>>/i_0/$, the exponential term in the equation that pertains to the reverse reaction becomes negligible and one obtains the Tafel relationship:

$$\eta_a = -1/\beta \frac{RT}{\not{z}F} (\ln/i/ - \ln i_0) \qquad (28)$$

This balance between the surface overpotential and ohmic drop can be characterized by the dimensionless ratio:

$$\delta = /i_{ave}/\frac{\not{z}Fro}{RT\kappa_\beta} \qquad (29)$$

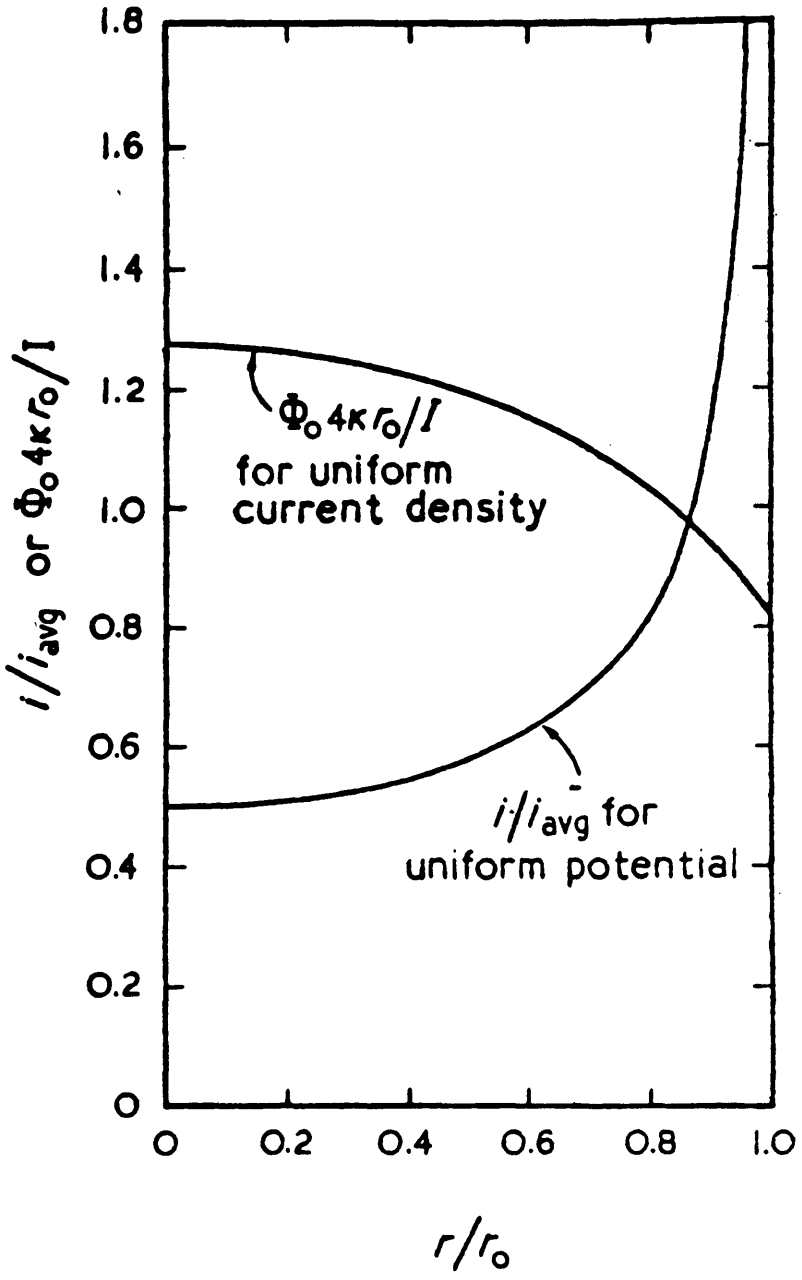

FIGURE 7. PRIMARY CURRENT DISTRIBUTION AND POTENTIAL DISTRIBUTION FOR UNIFORM CURRENT

As $\delta \rightarrow \infty$ then the current distribution approaches the primary distribution. Newman has generated a series of current distribution curves, for different values of $\beta\delta$, for the Tafel region, and this is shown in Figure 8.

As can be seen from Figure 8, the surface overpotential tends to make the secondary current distribution more nearly uniform than the primary distribution. Also it can be seen that the current density distribution becomes more uniform by increasing the conductivity of the solution and by decreasing the current to the disk.

If the current density is increased to a point where it becomes a significant fraction of the limiting current, then the effects of concentration overpotential should be included. The significance of the concentration overpotential can be shown through the relationship i/i_{Lim}. The limitation due to mass transport can be minimized by increasing the bulk concentration of the reactant, by increasing the rotational speed, by increasing the temperature and by decreasing the disk radius.

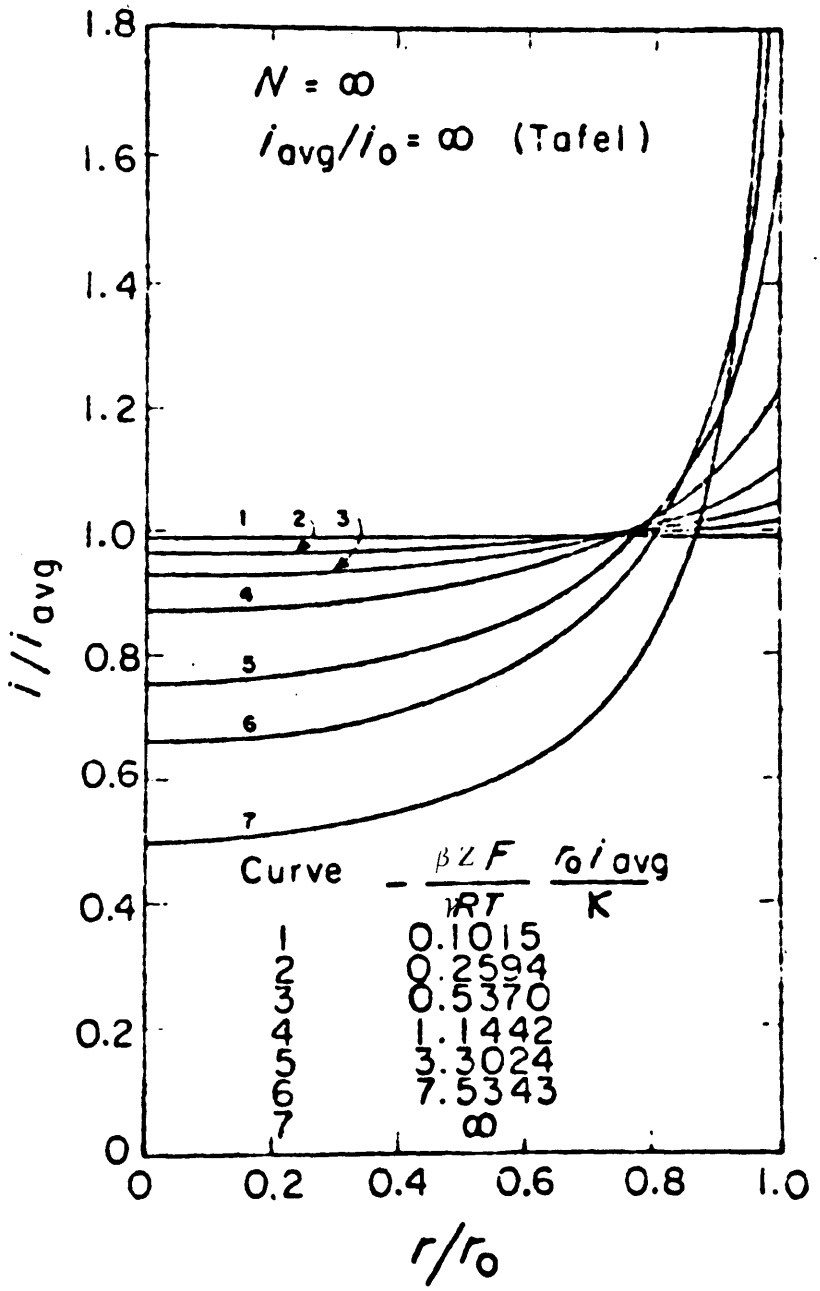

FIGURE 8. CURRENT DISTRIBUTION FOR TAFEL KINETICS

3. EXPERIMENTAL PROCEDURE

3.1 Hull Cell Arrangement

The initial plating was carried out using a basic Hull Cell arrangement in a 2 liter reaction vessel. The vessel was submerged in a constant temperature bath and a constant current was supplied to the electrodes using a Magna Model 4700M research potentiostat.

The results from the Hull Cell experiments gave a general feeling for the response of the system, although it became apparent that a different electrode arrangement would be necessary in order to control the various operating parameters that affected the deposit.

3.2 Rotating Disk Electrode Arrangement

A rotating disk arrangement was then set up as shown in Figure 9. The cathode was prepared from 1/4-inch copper plate with a 3/4-inch brass bushing that was drilled and reamed to 5/16-inch and soldered to the back. The electrode was then placed in a lathe and turned down to 3-inch diameter and faced providing a flat and true surface. The cathode was attached to the 5/16-inch shaft that was mounted to the reaction vessel lid through a two-piece polypropylene bushing. A pulley attachment was mounted to the top of the shaft and the rotational speed was set using a variable speed motor

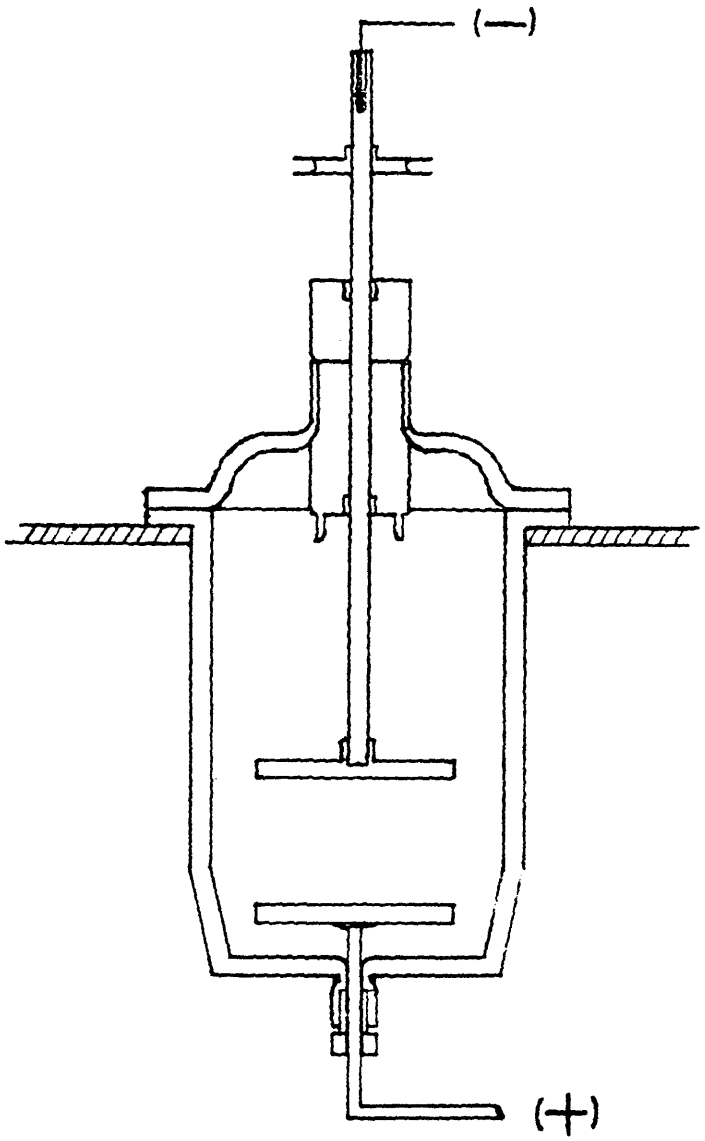

FIGURE 9. ROTATING DISK ARRANGEMENT

and checked with a PI digital tachometer.

A hole was drilled in the top of the shaft for a mercury pool reservoir that allowed electrical contact to cathode during operation. The anode was prepared from cobalt powder that was pressed and sintered into a 3-inch disk. The shaft and the back of the cathode and anode were coated with silicone rubber paint, and the entire vessel was submerged in a constant temperature bath.

These copper disks were polished, ultrasonically cleaned in dilute HCl and distilled water and then plated with nickel.

It then became necessary to change to a smaller disk because the 3-inch disk seemed somewhat impractical due to various reasons. First of all, the surface preparation was too time consuming. Also, this system seemed to be sensitive to concentration effects and a smaller disk would help prevent large changes in bath composition obtained from plating the large disks for long time periods.

One inch diameter disks were used with an oxidant concentration of .17m nitric acid and deposit adherence was checked using cellophane tape.

The disk size also came under consideration with regard to the optical measurements. Since a non-uniform current density is obtained, the size of the disk must be large enough so that the variation in current density over the area

that the optical measurements will be made should be less than 2 to 5%. This required a disk size slightly greater than one inch in diameter so a disk size of 1-1/3 inch was chosen for convenience. A teflon holder was prepared for the disks to insure a uniform mass transfer boundary layer as shown in Figure 10-C.

These disks were first polished to insure flatness and then plated with nickel. For most cases, the nickel was then polished down to 1 μm diamond, cleaned with benzene, ultrasonically cleaned in dilute hydrochloric acid and then distilled water until the surface became hydrophilic. After being removed from the final rinse the electrode was held face down so as not to disturb the film of water on the surface. The electrode was then carefully placed in the bath to prevent contact of the surface with the air.

Power to the electrode was provided with a Sorenson Model 40-12 programmable power supply. Plating current and time was controlled with an Apple-II micro-computer through a 12-bit, Burr-Brown digital to analog converter.

3.3 Optical Measurements

Optical measurements were made with a Gier-Dunkle solar reflectometer and a Gier-Dunkle infrared reflectometer. The emittance values obtained were for a spectral distribution similar to that obtained from a 100^{o}C blackbody and the ab-

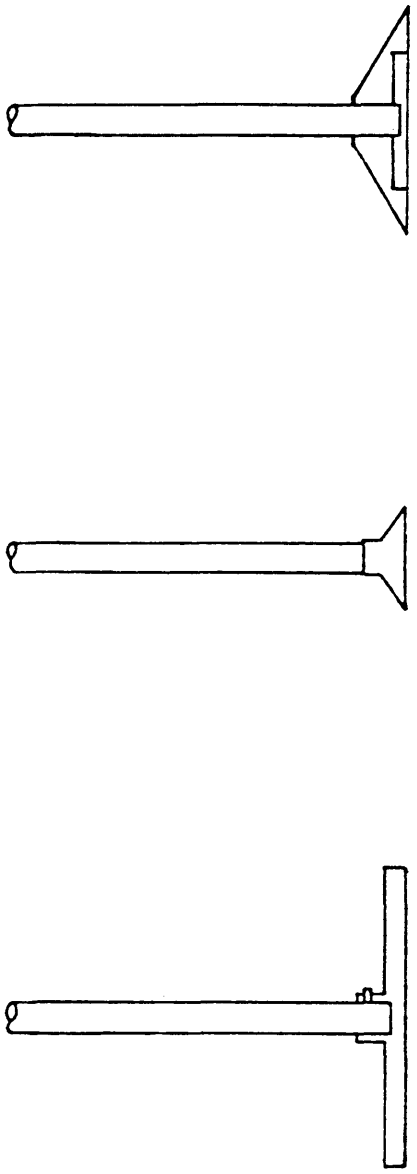

FIGURE 10. ELECTRODE CONFIGURATIONS

A - 3" Electrode

B - 1" Electrode

C - 1 1/3" Electrode with Teflon Sheath

sorbance values were for the spectral distribution of sunlight with an air mass of 2.

3.4 Thickness Measurements

Thickness measurements were performed in two ways. One way was to cross-section the electrode, mount it in casting resin or bakelight, polish down to .05 μm, and measure the thickness with a scanning electron microscope. The second way was to place a thin piece of graphics tape on the surface of the electrode before plating and then measure the thickness directly using a Ten-Core Alpha-Step Profiler that was accurate to 50 $\mathring{A}$.

3.5 Thermal Treatment

Plated samples were annealed at 250, 350 and 450^{o}C for 24 and 100 hour time periods. The first attempt at annealing resulted in spalling of the coating. This problem was overcome by increasing the nickel thickness to 25 μm.

3.6 X-Ray Measurements

X-ray measurements were performed with a Phillips XRG 3100 x-ray diffractometer using K copper radiation with a nickel filter. X-rays were taken of powder samples in a Debye-Scherrer arrangement and from directly placing the coated electrodes in the diffractometer.

3.7 Procedure for Determining Current Distribution

In order to estimate the current distribution obtained during the plating of black cobalt, a check was run on the current distribution obtained from metallic cobalt deposition. This was accomplished experimentally by placing a narrow piece of tape across the diameter of the disk and recording the time and total current. Thickness measurements were made, using the alpha-step profiler, as a function of radial distance. The thickness of the plate could be related to the number of coulombs passed per unit area which in turn could be related to the local current density.

4. EXPERIMENTAL DEVELOPMENT

4.1 Establishment of Bath Composition

The first step in the development of a plating system for black cobalt was to examine the commercial plating baths used in the electrodeposition of metallic cobalt. The most common baths included: sulfate bath, chloride bath, a Watts bath, a sulfamate bath, and a floroborate bath. The initial plating solution used was the Watts both with 319 g/lt $CoSO_4 \cdot 7H_2O$, 45 g/lt $CoCl_2 \cdot 6H_2O$, and 30 g/lt boric acid. The cobalt sulfate is the main source of cobalt ions, the cobalt chloride helps improve the conductivity and the boric acid is a leveling agent.

The first step was to relate the appearance of the deposit to large changes in current density. During some of these tests a fine black line was observed on the electrolyte-air interface. It was deduced that the difference between this interface and the bulk solution was that the interface had an influx of oxygen. So an oxidant was added to the bath and a black deposit was obtained.

The first oxidant that was tried was nitric acid at a molar concentration of .08. The first characteristic of the plating procedure that became apparent was that a blacker deposit was obtained at higher current densities, whereas a metallic cobalt deposit was obtained at lower current den-

sities. Also when the nitric acid concentration was increased a black deposit was obtained at lower current densities.

Hydrogen peroxide was then tried as an oxidant. Unacceptable deposits were obtained ranging from a pea-green to an olive-green color. The hydrogen peroxide used was fairly diluted so it might be possible to obtain black deposits with more concentrated H_2O_2, but since the H_2O_2 bath resulted in deposits having excessive spotting due to gas formation and since H_2O_2 has poor stability in water for extended periods of time, it was decided to concentrate further efforts using the nitric acid bath.

The next step was to test the affect of a different leveling agent. The same bath composition was used, only the boric acid was replaced with the same molar concentration of cobalt acetate. In order to obtain a black deposit it was necessary to use a higher nitric acid concentration and higher current densities relative to the previous bath. Also the deposit obtained appeared to be less black than that obtained previously using the boric acid and had poorer integrity.

A bath without any leveling agent was tested and it was found that this bath required higher oxidant concentrations and higher current densities in order to produce a black deposit.

The effect of the boric acid concentration on the de-

posit obtained was then tested using the three-inch rotating disk electrode arrangement. Tests were run at 350 rpm with .35 M nitric acid and at boric acid concentrations of .23, .35, .46, and .69 M (i.e. 10, 15, 20 and 30 g/lt).

The optimum boric acid concentration was .46 M, based on the minimum current density necessary to produce a black deposit and reduced smut formation.

Small amounts of ferrous sulfate were added to the bath with the intention of codepositing ferrous ions in the oxide. The ferrous sulfate did not seem to affect the plating process to any degree, although, after several hours, most of the ferrous sulfate added was oxidized and precipitated out of solution as ferrite hydroxide.

A small amount of molybdic acid (i.e. 4 g/lt) was added to the bath with the intention of improving the adherence. the result was that the molybdenum catalyzed the metallic cobalt reaction and made it nearly impossible to obtain a black deposit.

4.2 Identification and Standardization of Variables Affecting Deposit Characteristics

4.2.1 Effect of agitation

During the Hull Cell work, it was found that by slightly agitating the solution that; 1) the uniformity was greatly

improved, 2) the adherence was improved, 3) the smut formation was reduced, and 4) the current density necessary to produce the black was increased.

The use of the rotating disk electrode allowed control over the mass-transfer boundary layer and thereby providing reproducible and uniform agitation conditions.

The effect of the rotational speed was also checked. Tests were run at 100, 200, 350, and 500 rpm. The general tendency was that i_B increased with increasing rotational speed. However, the hard adhering black still occurred in the same current density range, independent of rotational speed (i.e. .60 to .80 kiloamps/m^2). The uniformity of the deposit improved with increasing rotational speed. Operating the disk at the high rotational speed (500 rpm) resulted in excessive spiraling due to gas formation at the electrode. Therefore, the rotational speed was fixed at 350 rpm for all of the following tests.

4.2.2 Effect of surface morphology

The effect of the surface morphology was checked by comparing the optical properties of films obtained with identical operating parameters on substrates with different surface roughnesses. The nickel-plated substrates were either sandblasted; sanded with 120, 240, 320, 400, or 600 grit emery paper; polished with 6 μm, 1 μm, or .05 μm diamond

or alumina abrasive, or left in the as-plated condition. The morphology of the as-plated substrates were a function of the current density used during the nickel deposition, resulting in a rougher surface with increasing current density.

The absorbance did not seem to be effected by the morphology except for being slightly greater on the as-plated substrates. The emittance varied between substrates, although in general, increased with increasing roughness. To insure uniformity the following samples were then polished down to a final polish consisting of 1 μm diamond paste on a nylon lap.

4.2.3 Effect of current density and oxidant concentrations

Once the bath composition was established, it was necessary to establish an effective range of oxidant concentrations and current densities. When the nitric acid concentration was greater than .2 M the film quickly dissolved after the power was shut off. It was also desirable to keep the current density below 5.0 kiloamps/m^2 to avoid high power requirements in commercial processes. Tests were run with different current density-oxidant concentration combinations and deposit appearance and integrity was observed.

4.3 Experimental Scheme Used to Correlate Oxidant Concentration, Current Density, Plating Time and Subsequent

Thermal Annealing with Optical Properties

Optical data was used to optimize the plating process with respect to oxidant concentration, current density, plating time, and subsequent thermal annealing.

Oxidant concentrations of .0167, .033, .050, .067, .100, .134, .167 m nitric acid were tested in the current density range of .70 to 4.50 kiloamps/m^2. The plating times used for the various oxidant concentration -- current density combinations, were designed to give various thicknesses in the range of .1 to 7 μm.

4.4 Use of Current Distribution as a Tool for Interpreting Data

The current distribution obtained from the metallic cobalt deposition was used as an aid in establishing the diagram for the type of deposits obtained versus the nitric concentration and current density. This was accomplished by measuring the radial distance on the disk where a specific deposit was obtained and relating that distance to an estimated local current density. Also when certain deposit characteristics were obtained within a definite radial distance range, that deposit could be reproduced for optical measurements.

5. DISCUSSION OF RESULTS

5.1 Factors Affecting Deposit Characteristics

The deposit obtained is a function of the oxidant concentration, the current density, and the agitation. At low current densities the deposit is metallic and as the current density increases the deposit becomes colored, giving a rainbow effect, and then results in a metallic black deposit. As the current density is increased further the deposit changes from a metallic black to a dull, flat black deposit with acceptable adherence and then into a loose, sooty black deposit.

By increasing the nitric acid concentration the current density necessary to obtain a black deposit, i_B, decreases rapidly up to an oxidant concentration of about .05 M nitric and then decreases slightly with increasing nitric acid.

The deposit obtained is also a function of the boric acid concentration. At lower concentrations i_B is very large and decreases with increasing boric concentration up to 20 g/lt, after this point i_B increases slightly with boric concentration and with excessive smut formation. This relationship is illustrated in Figure 13.

The surface pretreatment on the deposit obtained was found to be important. Poorly cleaned surfaces resulted in spotty and discontinuous deposits. Hydrophobic surfaces

also resulted in spotty deposits due to gas evolution. A study of the effect of surface pretreatment would be highly desirable and could help insure the ability to obtain reproducible results. The morphology of the substrate appears to have little effect on the deposit obtained as long as the surface pretreatment is the same. This is shown in Table III.

5.2 Current Distribution for Cobalt Deposition

In order to establish a diagram for the various deposits obtained, in relationship with the nitric concentration and the current density, the current distribution had to be estimated. This distribution was estimated from the current distribution obtained from the metallic cobalt deposition.

The results obtained from the profile measurements were compared to the theoretical current distribution obtained by assuming negligible concentration overpotential and Tafel kinetics. The experimental results seem to correlate well with the theoretical curve as shown in Figure 11.

Several points concerning Figure 11 need to be elaborated. First of all, the theoretical curve involves the assumption that the counter electrode is removed to infinity. In this system, the counter electrode and the working electrode were separated by a distance of 3 cm., which appears to be effectively the same as removing the counter-electrode to infinity. Also, the side reaction involving the evolution

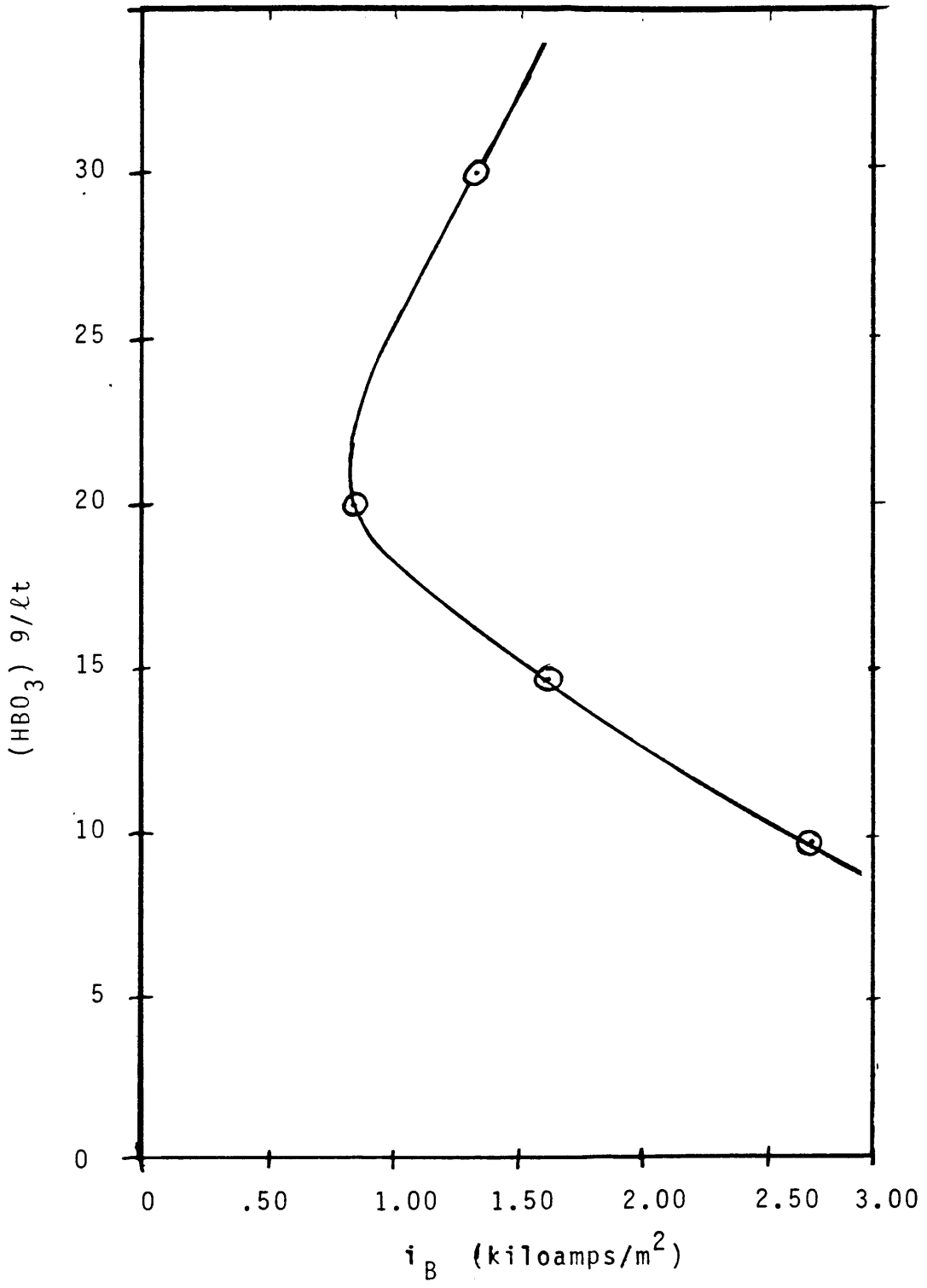

FIGURE 11. EFFECT OF BORIC ACID ON CURRENT DENSITY NECESSARY TO PRODUCE A BLACK DEPOSIT

of hydrogen, seems to be negligible. One final point is that the optical measurements were made in the area corresponding to the normalized radius of 0 to .4, resulting in a current density of:

$$i = .675\ i_{ave} \pm 4\%$$

Since the precise mechanism for the black cobalt reaction is not known at this time and since it involves the reduction of nitrate ions, it is difficult to predict the precise current distribution shown in Figure 11 seems to be a good approximation of the black cobalt current distribution by considering several observations. First of all, as the total current to the disk was increased, the radial distance, where a transition in the type of deposit was observed, decreased. When the local current density, at this transition, was estimated for different total currents, the values obtained were consistent.

Also from preliminary work it was known that a good adhering black deposit was obtained in a .067 M nitric acid within a specific current density range corresponding to 1.20 - 1.50 kiloamps/m^2. During the tests where the deposits were characterized as a function of radial distance, a deposit obtained in a .067 M nitric bath left a black adhering ring when rubbed. This ring had a definite inner and outer radius which represented a current density range of 1.20 -

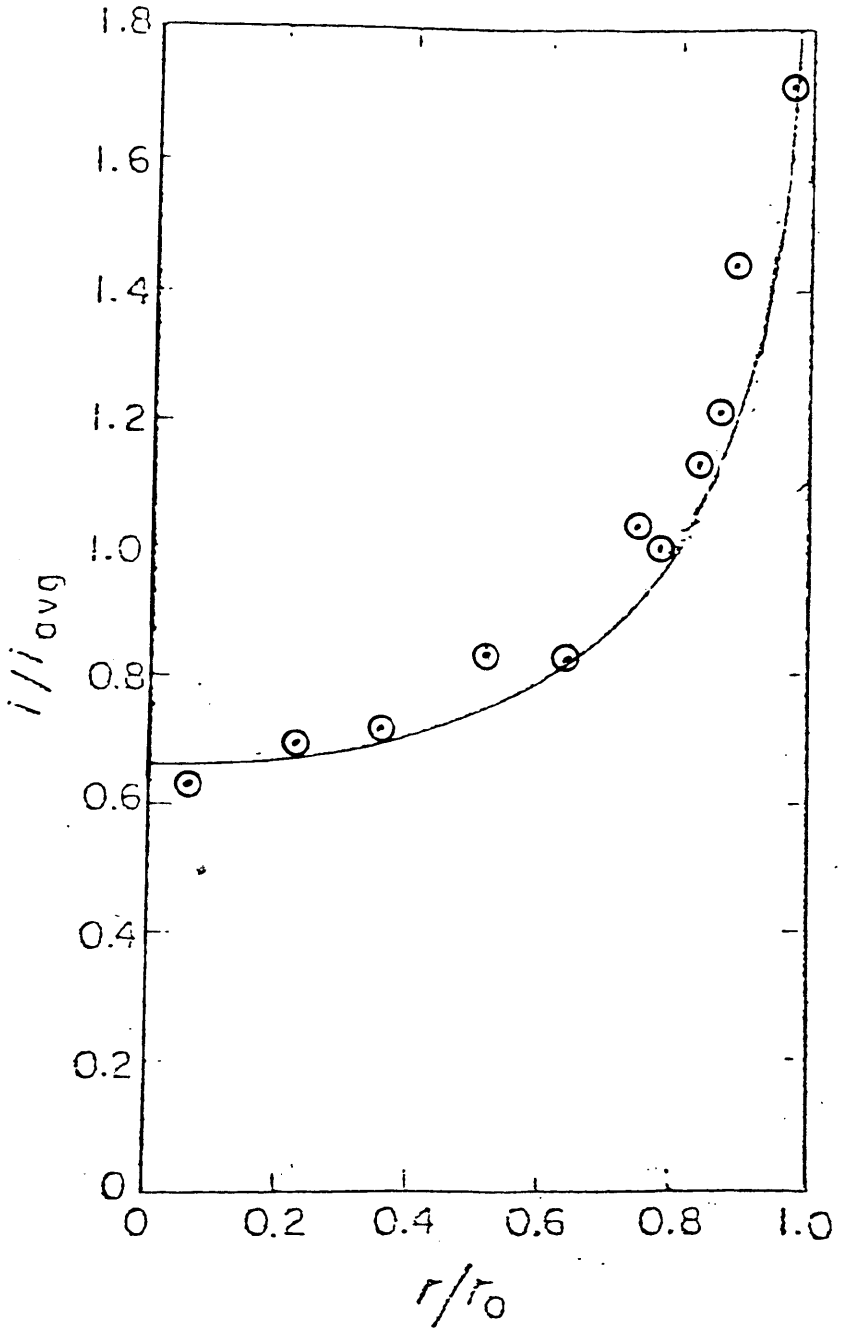

FIGURE 12. CURRENT DISTRIBUTION FOR COBALT ELECTRODEPOSITION

1.60 kiloamps/m^2 when related to the current distribution obtained from the metallic deposition.

5.3 Establishment of Deposit Characteristic Diagram

The deposit characteristic diagram obtained from relating deposit appearance and radial distance to the current distribution is shown in Figure 13.

This diagram shows the current density and oxidant concentration regions where the various deposits were obtained. This diagram corresponds to a Watts cobalt both with 20 g/lt boric acid and a rotational speed of 350 rpm. Also deposits obtained from other work seems to correlate well with this phase diagram.

5.4 Effect of Operating Parameters and Thermal Treatment on Film Thickness

Although extensive thickness measurements were planned, only a limited amount of data was obtained, especially for the as-plated thicknesses. However, several trends can be observed. First, in the metallic black region, the thickness obtained indicates that the density of the film is approximately that of cobalt metal. Also, as the current density increases the film thickness, per coulomb passed, increases slightly. In the blackest regions, the film thickness per coulomb passed increases significantly with increasing cur-

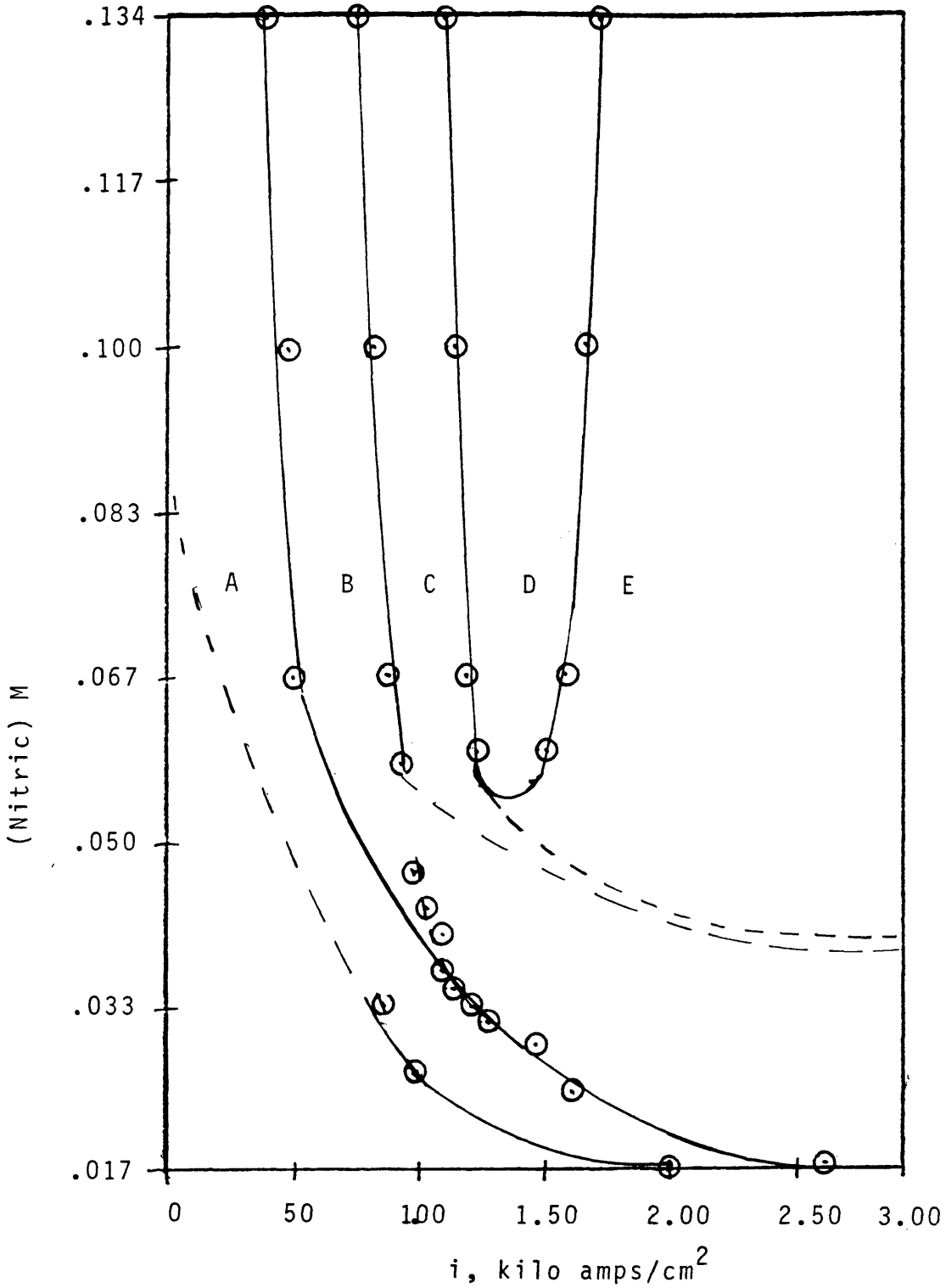

FIGURE 13. DEPOSIT DIAGRAM FOR BLACK COBALT ELECTRODEPOSITION

A. Metallic Cobalt
B. Colored Metal
C. Black
D. Adherent Dull Black
E. Sooty, Loose Black

rent density. For example, at an oxidant concentration of .033 M and for an equal amount of coulombs passed a deposit obtained at 3 amps will be 2.3 times thicker than a deposit obtained at 1 amp, as shown in Table I.

After annealing at 350°C for 24 hours the film thickness of most films decreased significantly. The effect of annealing on deposit thickness is shown in Table II. This was first apparent when films, initially black, became thin enough to cause spectral splitting (rainbow effect) or even to the point of transparency.

The exception of this generalization was for the colored metallic films, whose thickness increased on the order of 1.75 to 2 times the as-plated thickness. This is quite reasonable since these films were mostly cobalt metal to begin with and were then oxidized (i.e. the Pilling-Bedford ratio for CoO and Co_3O_4 is 1.76 and 2.00 respectively).

The thickness of several films in the black region were measured before and after annealing and these films showed a decrease in thickness upon annealing of 30 to 70%.

5.5 Results of X-ray Diffraction

X-ray diffraction data indicated that the coating was amorphous. After annealing at 350°C for 24 hours, the coating was still amorphous. After annealing at 650°C, low intensity peaks of CoO, Co_3O_4, and Co_2O_3 were obtained.

TABLE I. EFFECT OF DEPOSITION RATE ON DEPOSIT THICKNESS

A. Deposition rate for .017 M nitric solutions giving metallic black deposit

Sample #	i(amp/cm^2)	time(sec)	t, μm	t/(c/cm^2)
38	.375	3.9	.32 .39	.219-.267
39	.375	4.9	.45 .58 ave	.246-.32 .26
42	.427	3.9	.37-.47 ave	.22 -.28 .25
45	.480	1.95	.25-.28 ave	.27 -.30 .28
48	.534	.96	.124-.165	.24 -.32
49	.534	1.95	.242-.318	.23 -.30
50	.534	2.93	.434-.448	.28 -.29
51	.534	3.90	.678-.804 ave	.33 -.39 .30

(i.e. metallic cobalt deposition rate = .25 mm/(c/cm^2)

B. Deposition rate for .033 m nitric solutions giving black deposit

Sample #	i(amp/cm^2)	time(sec)	t, μm	t/(c/cm^2)
8	.107	3	.141	.44
10	.107	9	.507	.53
11	.107	6	.323	.50
			ave	.49
6	.321	9	3.25	1.12
7	.321	6.6	2.45	1.16
12	.321	3	1.02	1.06
			ave	1.12

TABLE II. EFFECT ON ANNEALING ON DEPOSIT THICKNESS

A. Effect of annealing on metallic black deposits

Sample #	Thickness, before	Thickness, after	% Change
39	.45	.55	+ 122
48	.125	.2	+ 160
51	.68	.85	+ 125
50	.4	.65	+ 160

B. Effect of annealing on black deposits

Sample #	Thickness, before	Thickness, after	% Change
56	.314	.1	- 68
64	.57	.4	- 30
60	.56	.30	- 46
68	1.8	.50	- 72

5.6 Consideration of Electrode Reactions

Further work needs to be done in order to elucidate the black cobalt reaction. However, it does involve the reduction of nitrate ions and in order for the nitrate ions to be reduced, there must be an ionic species available at the electrode surface capable of accepting the oxygen ions produced by the reduction of the nitrate ions. The combination of this adsorbed oxygen ion and a cobalt ion would seem more favorable than the combination of two hydrogen ions and the oxygen ion.

At low current densities, a metallic cobalt deposit is obtained due to the much greater concentration of cobaltous ions relative to the nitrate ions. When the current density is increased, the reduction of nitrate ions increases allowing the flux of nitrate ions to the surface due to diffusion to overcome the flux of nitrate ions away from surface due to electrical migration. Operating under these conditions results in the colored metallic and metallic black deposits. The color of the metallic deposit will depend on the relative reaction rates of the reduction of cobalt and the formation of the black deposit. The relative rates of these reactions will largely depend on the ratio of the cobaltous ions and nitrate ions at the electrode surface and on the substrate, as was observed from the experimental work.

When the current density is increased further, a total black deposit is obtained in which no cobaltous ions are reduced. This can be illustrated by considering the position on the Pourbaix diagram where the black cobalt deposition occurs, as shown in Figure 14. The potential at which a total black deposit is obtained falls in the potential range of +.07 to +.05 volts versus NHE and in a pH range of 1.0 to 5.0. In addition, it can be seen that the conditions at the electrode surface are not representative of the bulk electrolyte composition. However, it must also be understood that this diagram represents a simple Co-O-H system and not truly representative of the complex electrolyte system involved here.

As the current density is increased further, the limiting current for the reduction of nitrate ions is exceeded. It would therefore be necessary to reduce the nitrite ions even more to nitric oxide, nitrous oxide, or even to ammonium ions. The formation of nitric or nitrous oxides might also explain the formation of the loose sooty deposits at the higher current densities.

5.7 Emittance

The emittance of these films is a function of the film thickness, the emittance of the substrate, and the infrared

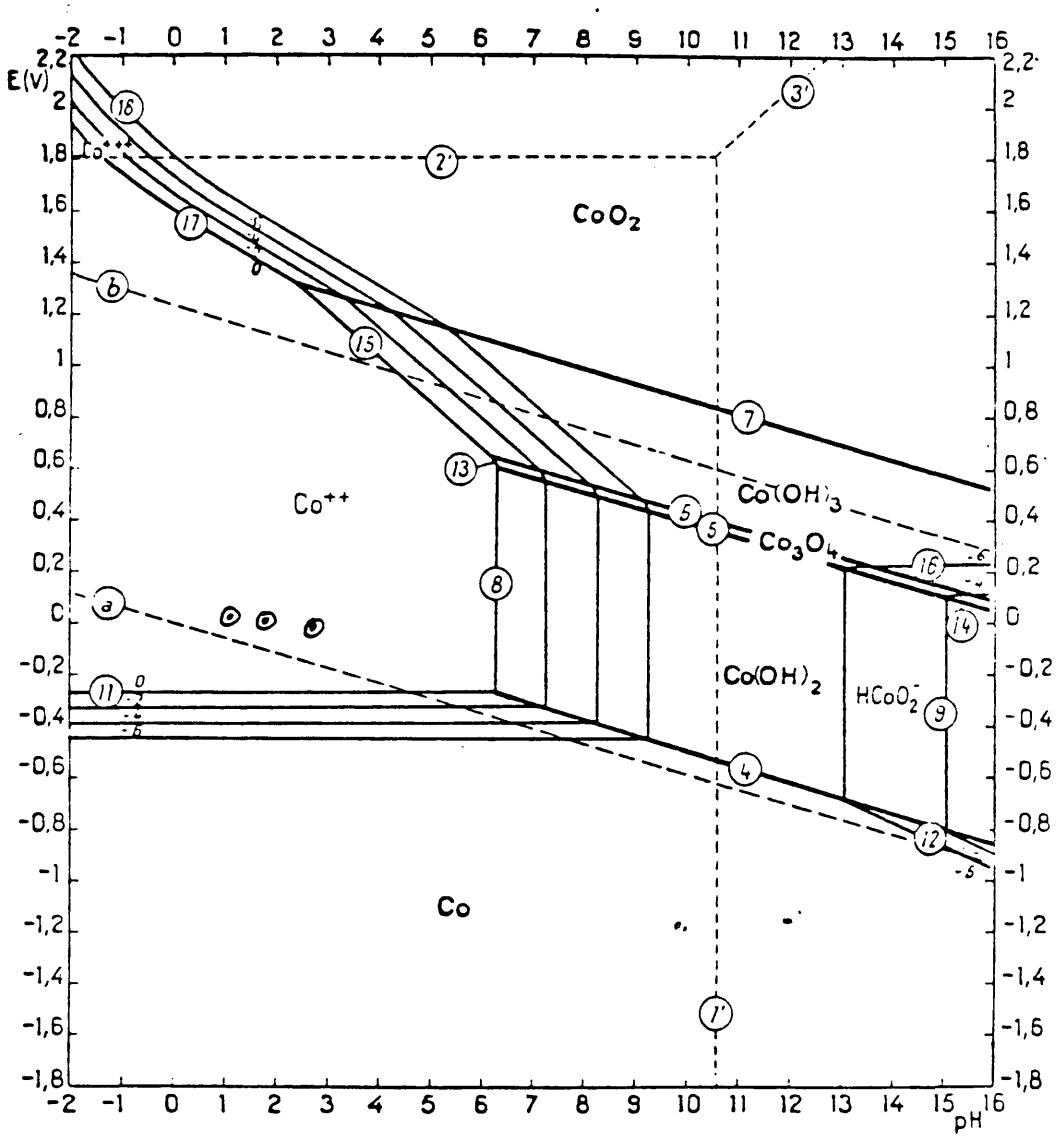

FIGURE 14. POURBAIX DIAGRAM FOR THE Co-O-H SYSTEM

absorbance characteristics of the material.

The emittance measurements were done with an IR spectral distribution similar to that of a 100°C black body whose half-peak height starts about 4 μm.

The emittance seems to increase linearly with thickness, also the surface roughness of the substrate seems to affect the emittance due to the greater emisivity of the uncoated surface as shown in Figure 15.

After annealing, the emittance drops significantly. In one case the emittance dropped from a value of .69 to .09 in one hour.

This drop in emisivity is primarily due to the decrease in thickness. However, the decrease in emittance is still substantially lower than can be accounted for by thickness alone. The IR absorption coefficient for a semi-conductor is largely affected by its free carrier concentration and low energy defect concentrations. Upon annealing the free carrier and defect concentrations establish themselves at an equilibrium value which is a function of the temperature and the oxygen partial pressure. This annealing decreases the IR absorption coefficient of the material and is indicated by a change in slope for an emittance versus thickness relationship as shown in Figure 16.

It can also be seen by Figure 16 that the emittance

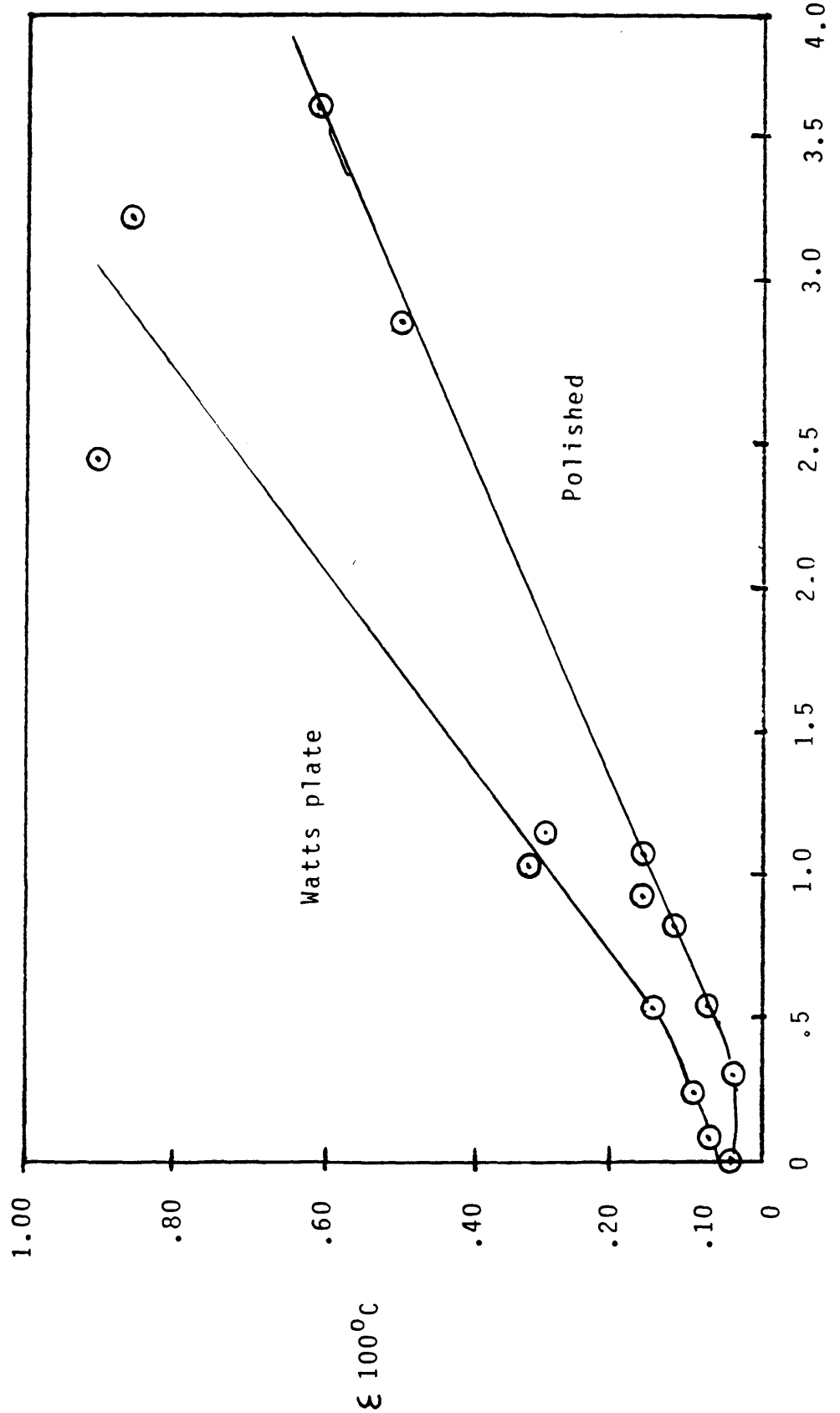

FIGURE 15. EMITTANCE VERSUS THICKNESS

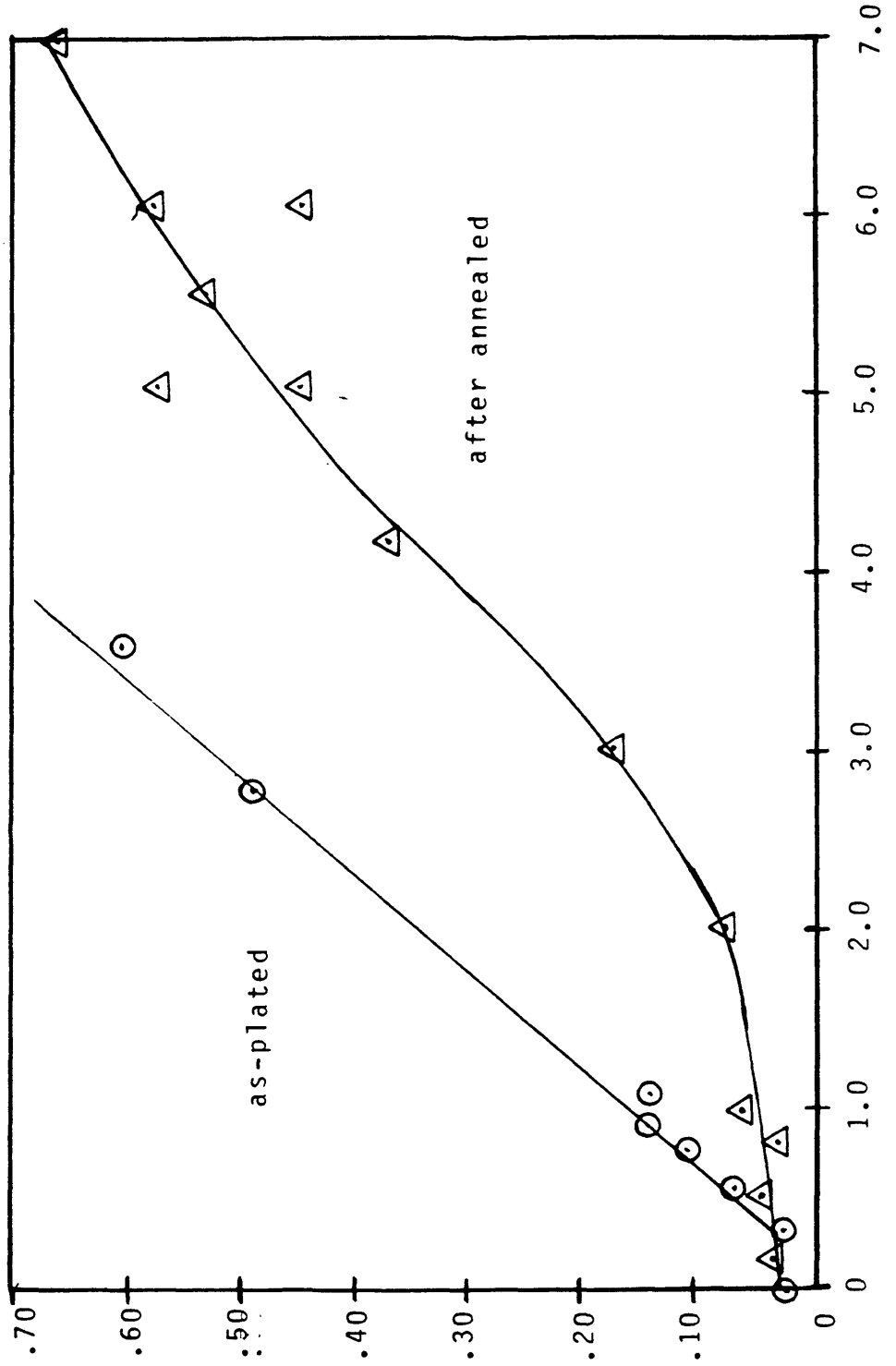

FIGURE 16. EFFECT OF ANNEALING ON EMITTANCE

rises sharply when the film thickness approaches the wavelength of the infrared spectrum used. After that point, the emittance is largely due to the emittance properties of the film material rather than the emittance properties of the substrate.

5.8 Absorbance

The absorbance of these films is a function of the thickness, the operating conditions, and the surface roughness of the substrate.

In general, the absorbance of the deposited material increases with increasing black properties (i.e. higher nitric concentration and higher current densities). This is what would be expected from visual inspection. Also the general trend is that absorbance increases with thickness up to a certain point. Many samples showed a decrease in absorbance with excessive thickness.

The more metallic samples had better absorbance at lower thicknesses and probably due to an interference effect. This absorbance also appears to change slightly depending on the substrate morphology. In one case, the absorbance improved slightly when the substrate was polished down to 1 μm diamond when compared to a substrate sanded with 600 grit; whereas for a slightly thicker film under the same conditions the sanded substrates showed better absorbances and emittances.

When the nickel substrate was plated as high current densities, the nickel surface appeared white and microscopically rough. When absorbance measurements were compared between this "as-plated" nickel surface and an identical coating on a polished surface, the absorbance of the as-plated samples were consistantly 2% higher.

When these films were annealed, the solar absorbance dropped substantially. This drop in absorbance is mainly due to the decrease in thickness and considering a 50% to 70% change in thickness, this change can mainly be attributed to a thickness phenomena. However, even for some films of excessive thickness, the absorbance still dropped between 2% to 4% and this is probably due to the annealing out of color centers and other defects or a change in chemical composition.

As a consequence the best films obtained so far have a solar absorbance after annealing of .90 to .93 and emittance values of about .10. (The optical data for various operating conditions is tabulated in the Appendix).

5.9 Optimized Coating

An optimum coating should not only have a high solar absorbance and a low thermal emittance, but it should also have good adherence, good integrity, stable at high temperatures, and be easily reproduced.

Films with acceptable adherence have been obtained in

definite current density ranges for a given oxidant concentration. Operating conditions should be in this range so that plated receivers can be practically handled.

At low pH, the deposits dissolve after the power is shut off. This will limit the nitric acid concentration used to at least .16 M and preferably to .07 to .1 M nitric. Low nitric concentrations result in high current densities necessary to produce a black coating and at the expense of good optical properties.

To date, the optimum conditions to fulfill these requirements seems to be in the range of .07 to .1 M nitric acid at a current density of 1.20 to 1.60 kiloamps/m^2 with an after annealed thickness of about 2 μm.

6. CONCLUSIONS

The properties of electrodeposited black cobalt can be controlled through the proper operating conditions. The absorbing properties of the deposit can be increased by increasing the oxidant concentration and/or the current density. Acceptable adhering films can be obtained with proper agitation and operating in an appropriate current density range. In general, the solar absorbance and infrared emittance increase with increasing thickness. Therefore, proper control over deposit thickness is needed to insure selectivity. However, the film thickness collapses significantly upon annealing and might be attributed to a decrease in porosity, although a change in chemical composition is more likely to be the reason.

To date the optimum operating conditions have been in the range of .07 to .1 M nitric acid and at a current density of 1.20 to 1.60 kiloamps/m^2. Films obtained with these operating conditions have had acceptable adherence and an after-annealed solar absorbance of .91 to .93 with an infrared emittance of .10 to .20.

Black cobalt seems to be a good candidate for the realization of a high temperature selective absorber coating. Obtaining black cobalt directly through electro-deposition provides the economic advantage of in-situ annealing.

7. FUTURE WORK

Areas of future work that need to be pursued are: identification of the chemical composition of the film, determination of the reaction mechanism, a study of the surface pretreatment, extended annealing times and temperatures, the effect of alloying additions on the optical properties and thermal stability, and the development of a commercial process.

Determination of the chemical composition of the as-plated film would be the first step in determining the reaction mechanism. It would also give an understanding of the change in optical properties upon annealing. Depth profiling of the after annealed films could tell if the oxide had reached thermal equilibrium, it would give an indication of the extent of the oxidation of the substrate, and the possible alloying of the substrate with the deposit.

Once the reaction product is known, one can write the possible chemical equations involving the species present for the reaction and the reaction product obtained.

By using KNO_3 as the oxidant and by running several polarization curves at various oxidant concentrations, one should be able to obtain the order of the reaction with respect to the nitrate concentration. Likewise, by adjusting the pH with sulfuric acid, one should be able to obtain the

reaction order with respect to the hydrogen ion concentration.

One problem that might be encountered is the effect of the competing reduction reactions. However, if the number of coulombs passed are recorded followed by potentiostatically stripping of the deposit in an alkaline solution with a coulomb counter, one can estimate the extent of the competing reactions during the deposition.

During this work, the bath composition should be analyzed using pology, in order to identify possible complexes such as cobalt nitrates or nitrites. In addition, care must be taken in interpreting the results with respect to the effects of ohmic, kinetic, and concentration overpotentials on the current distribution.

The absorbance of the oxide and the thermal stability can be improved by the addition of alloying agents. It has been shown (20) that, by partial substitution of other trivalent cations (Al^{+3}, Cr^{+3}, etc.) for the Co^{+3} in Co_3O_4, the spinel can be stabilized above 900°C with respect to its dissociation to the monoxide. Also if rare earth elements are added to the oxide, improved absorption would occur due to the characteristic absorption of the rare earths and from lattice distortion.

Further work needs to be done in evaluating the thermal stability of the system. Annealing times and temperatures

obtained so far are far from being adequate for evaluating long term thermal stability.

Once the mechanism is determined and the coating is shown to be stable during operation, work will need to be done in developing a commercial plating process for black cobalt. Important considerations in this respect will be: bath stability, reproducibility, agitation control, and control over current distribution and mass transport effects.

APPENDIX

TABLE III. EFFECT OF SUBSTRATE MORPHOLOGY ON OPTICAL PROPERTIES

Plating conditions: .033 m nitric, 100 milliamps/cm^3 for 6 seconds

Sample #	Surface	α	ε
24	Sandblast	.80	.67
25	120 grit	.93	.10
26	320 grit	.94	.13
27	600 grit	.93	.07
29	.05 μm	.93	.06
30	1 μm	.94	.05
31	1 μm	.96	.05
32	1 μm	.96	.07
33	1 μm	.95	.06
34	6 μm	.94	.07

Plating conditions: .067 m nitric, 100 milliamps/cm^2 for 14 seconds

Sample #	Surface	α	ε
14	Sandblast	.91	.15
15	60 grit	.92	.13
16	240 grit	.93	.12
17	400 grit	.94	.11
18	15 µm	.94	.08
19	.05 µm	.93	.10
20	1 µm	.93	.13
21	1 µm	.92	.15
22	1 µm	.92	.13
23	1 µm	.92	.18

Plating conditions: .067 m nitric, 100 milliamps/cm^2 for 14 seconds

Sample #	Surface	α	ε
138	320 grit	.93	.11
104	400 grit	.92	.19
152	600 grit	.90	.14
127	15 µm	.92	.12
144	6 µm	.89	.14
113	1 µm	.92	.12
101	badly pitted	.92	.12
105	80 m amp/cm^2 Watts Ni	.93	.14
141	100 m amp/cm^2 Watts Ni	.94	.15
119	150 m amp/cm^2 Watts Ni	.94	.14
115	200 m amp/cm^2 Watts Ni	.94	.17

DATA IN SUPPORT OF FIGURE 11

.35 M nitric acid and 350 rpms

(Boric Acid) g/lt	M	i_B (milliamps/cm^2)
10	.23	270
15	.34	160
20	.46	80
30	.68	137

DATA IN SUPPORT OF FIGURE 12

Electrode Radius - 17.21 mm

Electrode area (minus tape) - 8.48 cm^2

Total current - 1.0 amp

Total time - 1.0 min

Average current density - .1179 amp/cm^2

$Amp\text{-}min/cm^2$ to give 1 KÅ - 4.831×10^{-3}

r(mm)	t_1(KÅ)	t_2(KÅ)	t_{ave}(KA)	i_r(amp/cm^2)	r/r_o	i_r/i_{ave}
16.35	42.0	42.0	42.0	.2029	.962	1.72
15.35	35.5	35.5	35.5	.1715	.892	1.46
14.69	25.9	33.5	29.7	.1435	.854	1.21
14.16	30.5	24.5	27.5	.1329	.823	1.13
13.50	21.5	27.5	24.5	.1184	.784	1.00
13.14	28.5	22.5	25.5	.1232	.764	1.05
10.93	18.4	22.0	20.2	.0976	.635	.828
8.67	22.5	18.4	20.4	.0986	.504	.856
6.21	16.8	18.5	17.6	.0850	.361	.721
3.75	17.5	16.75	17.1	.0826	.218	.700
1.23	16.0	15.5	15.75	.0761	.071	.645

r_o = 1.72 cm

ω = 36.65 rad/s

ν = .192 cm^2/s

a = .510

D = $.7 \times 10^{-5}$ cm^2/s

n = 2

$\not{z}$ = -2

$i_o = 2 \times 10^{-3}$ amps/cm^2

$i_L = \pm .620\, \nu FD^{2/3}\, \nu^{-1/6}\, \omega^{1/2}$ $\quad C = .462$ amp/cm^2

$F = 96495.4$ coul/eq

$C_B = 1.325 \times 10^{-3}$ moles/cm^3

$R = 8.3\ 1\ 5$ Joul/mole-deg

$T = 298^oK$

$\kappa = .425$ mho/cm

$Re = r^2\omega/\nu = 565$

$i_{ave}/i_L = .23$

When $/i/ >> i_o$, then Tafel kinetics apply described by the dimensionless parameter δ :

$$-\beta\delta = -\beta\, /i_{ave}/\frac{\nu Fro}{RT\kappa} = 16.8$$

DATA IN SUPPORT OF FIGURE 13

i_2 = approximate current density where the colored metal appears (milliamps/cm^2)

i_2 = current density where first black appears

i_3 = current density range where a hard adherent deposit is obtained (milliamp/cm^2)

(Nitric)M	i_2	i_2	i_3
.0167	200	260	---
.0234	100	160	---
.030	---	147	---
.0317	---	120	---
.0334	90	117	---
.0351	---	111	---
.0367	---	110	---
.040	---	110	---
.0434	---	109	---
.0468	---	103	---
.0501	---	99	---
.0585	---	95	120-150
.0668	50	90	115-155
.1002	50	80	110-160
.1336	40	75	110-

DATA IN SUPPORT OF FIGURE 14

E(SCE), volts	pH
- .1745	1.0
- .1750	2.0
- .1760	3.0

DATA IN SUPPORT OF FIGURE 15

Emittance of as-plated black cobalt with .033 M nitric on a polished nickel surface.

Sample #	Thickness μm	α_s	ε 100°C
5	uncoated	---	.03
56	.314	78	.03
57	.524	.64	.08
58	.734	.66	.12
59	.943	.61	.16
159	1.12	.90	.15
157	2.88	.92	.50
158	3.6	.92	.61

Emittance of as-plated black cobalt with .033 M nitric on an unpolished nickel surface

Sample #	Thickness μm	α_s	ε 100°C
8	.14	.84	.06
11	.323	.92	.09
10	.507	.94	.14
12	1.02	.96	.33
9	1.28	.94	.26
7	2.45	.96	.92
6	3.25	.95	.86

DATA IN SUPPORT OF FIGURE 16

Data for as-plated emittances are taken from data in support of Figure 16 for polished surface.

Emittance of black cobalt samples after annealing at 350°C for 24 hours.

Sample #	Thickness μm	α	ε100°C
107	9.2 edge	.88	.43
118	2.0	.89	.12
166	4.2	---	.38
124	6.0	.91	.58
168	5.0	.87	.45
167	3.0	.90	.18
170	7.0	.93	.65
169	5.5	.91	.55
171	1.0	.87	.07
174	5.0	.91	.58
176	6.0	.89	.46
97	.78	.72	.03
82	.45	.85	.06
77	.15	.79	.04

TABLE IV

Optical properties of films obtained with different operating parameters.

Annealing temperature = $350^{o}C$

Current density = $.675\ i_{ave}$

SAMPLE #	$(NO_3)M$	i kiloamps/m^2	time(sec)	before		after 1 hr		after 24 hrs	
				α	ϵ	α	ϵ	α	ϵ
36	.0167	2.539	2	.78	.07	.85	.06	.77	.07
37	.0167	2.539	3	.71	.11	.84	.07	.70	.08
38	.0167	2.539	4	.72	.14	.74	.08	.64	.08
39	.0167	2.539	5	.74	.18	.71	.09	.61	.08
40	.0167	2.902	2	.77	.08	.79	.05	.69	.05
41	.0167	2.902	3	.77	.14	.69	.06	.61	.07
42	.0167	2.902	4	.81	.18	.69	.08	.59	.07
43	.0167	2.902	5	.76	.22	.75	.10	.59	.07
44	.0167	3.265	1	.69	.06	.83	.05	.72	.06
45	.0167	3.265	2	.79	.09	.79	.05	.78	.07
46	.0167	3.265	3	.81	.12	.64	.06	.60	.07
47	.0167	3.265	4	.83	.23	.71	.09	.60	.07
48	.0167	3.628	1	.80	.08	.79	.05	.75	.05
49	.0167	3.628	2	.80	.10	.82	.06	.72	.09
50	.0167	3.628	3	.84	.18	.64	.06	.58	.06
51	.0167	3.628	4	.88	.27	.75	.12	.70	.09

SAMPLE #	$(NO_3)M$	i kiloamps/m^2	time(sec)	before		after 1 hr		after 24 hrs	
				α	ϵ	α	ϵ	α	ϵ
52	.0334	.580	8	.74	.04	.78	.04	.68	.05
53	.0334	.580	12	.66	.06	.87	.05	.86	.04
54	.0334	.580	16	.88	.06	.64	.05	.72	.05
55	.0334	.580	20	.65	.12	.86	.08	.66	.08
56	.0334	.726	6	.78	.03	.81	.04	.73	.04
57	.0334	.726	10	.64	.08	.83	.06	.75	.07
58	.0334	.726	14	.66	.12	.78	.07	.69	.07
59	.0334	.726	18	.61	.16	.84	.08	.70	.07
60	.0334	1.016	4	.86	.03	.80	.04	.65	.06
61	.0334	1.016	8	.77	.10	.80	.06	.75	.05
62	.0334	1.016	11	.78	.16	.79	.08	.65	.07
63	.0334	1.016	14	.69	.20	.82	.08	.65	.08
64	.0334	1.306	4	.86	.04	.73	.04	.64	.04
65	.0334	1.306	6	.86	.08	.72	.06	.64	.05
66	.0334	1.306	9	.90	.16	.72	.08	.63	.07
67	.0334	1.306	11	.89	.24	.72	.08	.70	.08
68	.0334	1.016	20	.65	.22	.85	.08	.70	.06

SAMPLE #	$(NO_3)M$	i kiloamps/m^2	time(sec)	before		after 1 hr		after 24 hrs	
				α	ϵ	α	ϵ	α	ϵ
158	.0334	2.177	10	.92	.61	.89	.34	.77	.29
157	.0334	2.177	8	.92	.50	.88	.15	---	.16
159	.0334	2.177	3.1	.90	.15	.85	.08	.87	.07
160	.0334	2.539	2.71	.93	.15	.88	.06	.87	.07
161	.0334	2.539	7.714	.93	.74	.90	.30	.78	.28
162	.0334	2.902	2.373	.92	.15	.90	.06	.89	.07
163	.0334	2.902	6.75	.93	.89	.92	.28	.80	.25

SAMPLE #	$(NO_3)M$	i kiloamps/m^2	time(sec)	before		after 1 hr		after 24 hr	
				α	ϵ	α	ϵ	α	ϵ
69	.0501	.580	8	.88	.05	.74	.04	.82	.11
70	.0501	.580	12	.78	.06	.67	.04	.84	.14
71	.0501	.580	16	.80	.07	.77	.05	.74	.07
72	.0501	.580	20	.78	.09	.77	.05	.79	.09
73	.0501	.726	6	.88	.04	.87	.04	.87	.10
74	.0501	.726	10	.80	.04	.84	.04	.69	.05
75	.0501	.726	14	.89	.05	.69	.04	.75	.06
76	.0501	.726	18	.90	.08	.75	.05	.77	.07
77	.0501	1.016	4	.73	.04	.76	.03	.79	.04
78	.0501	1.016	8	.93	.05	.87	.04	.73	.06
79	.0501	1.016	11	.94	.07	.88	.04	.84	.05
80	.0501	1.016	14	.96	.23	.84	.06	.83	.06
81	.0501	1.306	4	.86	.05	.94	.05	.76	.09
82	.0501	1.306	6	.90	.14	.90	.04	.85	.08
83	.0501	1.306	9	.95	.31	.92	.06	.89	.06
84	.0501	1.306	11	.95	.52	.93	.09	.91	.11

SAMPLE #	$(NO_3)M$	i kiloamps/m^2	time(sec)	before		after 1 hr		after 24 hr	
				α	ϵ	α	ϵ	α	ϵ
85	.0668	.580	8	.80	.04	.79	.04	.75	.05
86	.0668	.580	12	.88	.04	.78	.04	.76	.04
87	.0668	.580	16	.93	.04	.75	.04	.65	.04
88	.0668	.580	20	.91	.05	.71	.04	.75	.05
89	.0668	.726	6	.71	.04	.81	.04	.71	.04
90	.0668	.726	10	.93	.05	.84	.04	.70	.04
91	.0668	.726	14	.96	.09	.87	.04	.87	.06
92	.0668	.726	18	.95	.10	.79	.05	.81	.17
93	.0668	1.016	4	.78	.04	.76	.04	.88	.09
94	.0668	1.016	8	.93	.13	.86	.04	.88	.04
95	.0668	1.016	11	.95	.26	.89	.05	.87	.05
96	.0668	1.016	14	.96	.49	.92	.07	.93	.10
97	.0668	1.306	4	.87	.07	.81	.04	.72	.03
98	.0668	1.306	6	.94	.20	.87	.04	.87	.08
99	.0668	1.306	9	.96	.46	.92	.07	.92	.13
100	.0668	1.306	11	.96	.69	.90	.10	.92	.12

SAMPLE #	$(NO_3)M$	i kiloamps/m^2	time(sec)	before		after 1 hr		after 24 hr	
				α	ϵ	α	ϵ	α	ϵ
102	.0668	.580	25	.91	.73	.88	.46	.86	.32
103	.0668	1.306	8	.94	.64	.90	.11	.92	.11
106	.0668	1.45	6	.91	.75	.89	.39	.88	.30
108	.0668	1.596	7	.92	.77	.92	.54	.91	.42
175	.0668	1.596	10	.94	.87	.92	.40	.93	.38
120	.0668	1.45	25	.95	.82	.93	.75	---	.72

SAMPLE #	$(NO_3)M$	i kiloamps/m^2	time(sec)	before		after 1 hr		after 24 hr	
				α	ϵ	α	ϵ	α	ϵ
109	.1002	.508	17.1	.94	.22	.84	.05	.88	.05
111	.1002	.508	25.71	.94	.42	.89	.11	.92	.12
112	.1002	.508	34.29	.94	.46	.88	.10	.91	.10
118	.1002	.508	42.86	.95	.65	.88	.12	.89	.12
114	.1002	.8707	10	.93	.31	.82	.06	.86	.07
116	.1002	.8707	15	.95	.68	.81	.11	.88	.12
117	.1002	.8707	20	.95	.85	.87	.46	.91	.42
107	.1002	.8707	25	.94	.82	.85	.47	.88	.43
121	.1002	1.233	7.06						
122	.1002	1.233	10.59	.95	.86	.89	.55	.92	.51
123	.1002	1.233	14.12	.91	.14	.83	.05	.86	.05
124	.1002	1.233	17.65	.93	.82	.88	.61	.91	.58
125	.1002	1.596	5.45	.94	.56	.82	.11	.85	.11
126	.1002	1.596	8.18	.94	.85	.90	.46	---	.43
128	.1002	1.596	10.91	.91	.84	.87	.76	.91	.75
166	.1002	1.596	13.64	.95	.84	.91	.62	---	.58

SAMPLE #	$(NO_3)M$	i kiloamps/m^2	time(sec)	before		after 1 hr		after 24 hr	
				α	ϵ	α	ϵ	α	ϵ
129	.1336	.508	17.1	.85	.09	.80	.05	.89	.06
130	.1336	.508	25.71	.89	.23	.83	.08	---	---
131	.1336	.508	34.29	.94	.65	.85	.12	.90	.13
167	.1336	.508	48.86	.94	.72	.86	.18	.90	.18
132	.1336	.8707	10	.91	.32	.82	.08	.89	.08
133	.1336	.8707	15	.95	.75	.81	.21	.88	.18
134	.1336	.8707	20	.95	.85	.83	.46	.87	.38
168	.1336	.8707	25	.95	.84	.87	.49	.87	.45
135	.1336	1.233	7.06	.95	.54	.80	.13	---	---
136	.1336	1.233	10.59	.95	.83	.86	.38	.92	.31
137	.1336	1.233	14.12	.95	.86	.87	.55	---	---
169	.1336	1.233	17.65	.95	.83	.87	.58	.91	.55
139	.1336	1.596	5.45	.94	.55	.85	.15	.90	.11
140	.1336	1.596	8.18	.95	.87	.90	.50	.93	.46
142	.1336	1.596	10.91	.95	.86	.90	.62	.93	.58
170	.1336	1.596	13.64	.95	.85	.91	.65	.93	.65

SAMPLE #	$(NO_3)M$	i kiloamps/m^2	time(sec)	before		after 1 hr		after 24 hr	
				α	ϵ	α	ϵ	α	ϵ
143	.167	.508	17.1	.80	.08	.74	.05	.86	.04
145	.167	.508	25.71	.92	.17	.86	.06	.90	.03
146	.167	.508	34.29	.94	.23	.85	.07	.91	.07
171	.167	.508	48.86	.95	.30	.85	.07	.87	.07
147	.167	.8707	10	.88	.14	.78	.05	.85	.03
148	.167	.8707	15	.94	.56	.82	.13	.90	.11
149	.167	.8707	20	.95	.85	.82	.42	.90	.40
172	.167	.8707	25	.95	.85	.83	.49	.90	.42
150	.167	1.233	7.06	.92	.36	.78	.07	.86	.09
151	.167	1.233	10.59	.95	.81	.84	.21	.90	.20
153	.167	1.233	14.12	.95	.86	.84	.48	---	---
176	.167	1.233	17.65	.95	.82	.85	.51	.89	.46
154	.167	1.596	5.45	.95	.59	.84	.12	.86	.12
155	.167	1.596	8.18	.95	.84	.87	.40	.90	.40
156	.167	1.596	10.91	.95	.86	.88	.58	---	---
174	.167	1.596	13.64	.95	.83	.89	.60	.91	.58

8. REFERENCES

1. Tabor, H., Research on Optics of Selective Surfaces. Contract AF 61 (052)-279, (1963).

2. Sowell, R.R. and R.B. Pettit, Thermal Aging of Electro-Deposited Black Chrome, Proceedings D.O.E./D.S.T. Thermal Power Systems Workshop on Selective Absorber Coatings. Dec. 6-8, 1977.

3. Private communication with P. Call, Solar Energy Research Institute, 1979.

4. Kokoropoulous, P., E. Salam, and F. Daniels. Solar Energy, 3, 19 (1959).

5. Srivastava, R.D., and S. Kumar, Plating, pp. 487-490, May, (1973).

6. Lindsay, J.H. II, and H.J. Read, Plating, pp. 497-503, May, (1970).

7. Srivastava, R.D. and S. Kumar, Acta Chemica, Hungary, 78, (2), pp. 139-148 (1973).

8. Sard, R., C.D. Schwartz, and R. Weil, Electrochem Soc., pp. 113, 424, (1966).

9. Morral, F.R., Plating, pp. 693-701, June 1977.

10. Byers, H.G., J. Am. Chem. Soc., 30, 1718 (1908).

11. Byers, H.G. and C.W. Thing, ibid. 33, 389 (1927).

12. El-Wakkad, S.E.S. and A. Aickling, Trans. Faraday Soc., 46, 1820 (1950).

13. Cowling, R.D. and A.C. Riddiford, Electrochim Acta, 14, 981 (1969).

14. Sato, N. and T. Ohtsuka, J. Electrochem. Soc., 125, 1735 (1978).

15. Eisemongy, M.M., Y.A. Elewady and M.M. Gouda, J. Electro-anal. Chem., 81, pp. 113-121, (1977).

16. German Patent No. 25 56 716. Assignee: Philips Patenverwaltung GMBH, inventor Heinz Scholz.

17. Riddiford, "The Rotating Disk System", Advances in Electro-Chemistry and Electrochemical Engineering, 4, pp. 47-116, (1966).

18. Levich, V.G., Acta Physiocochem U.S.S.R. 17 257 (1942).

19. Newman, J., J. Electrochem. Soc., 113, 1235 (1966).

20. Badard, A.M. and J.M. Paris, Comptes-Rendus, 258, 2085 (1964).